Title: Immune–tracheal intercellular signalling coordinates the muscle injury response in *Drosophila*

Authors: Nourhene Ammar[1], Olivier Josse[1], Aurélien Guillou[1], Jessica Perochon[2] and Hadi Boukhatmi[1]*

[1] Institut de Génétique et Développement de Rennes (IGDR), Université de Rennes, CNRS UMR6290, Rennes, France.

[2] Institute of Cancer Sciences−University of Glasgow, Wolfson Wohl Cancer Research Centre, Glasgow, UK.

* Corresponding author: hadi.boukhatmi@univ-rennes.fr

Summary

Effective tissue adaptation to damage requires precise coordination among diverse cell types. In skeletal muscle, the cellular and molecular mechanisms that orchestrate this coordination remain incompletely understood. Here, we identify adult *Drosophila* immune cells, hemocytes, as central organizers of post-injury muscle repair. Muscle damage triggers rapid recruitment of hemocytes to affected fibers. Hemocyte-derived FGF-like ligand Branchless (Bnl) activates FGF/FGFR signalling on vascular-like tracheal cells, guiding their localized expansion toward injured regions. In parallel, hemocytes deposit extracellular matrix (ECM) components, including Collagen IV, which accumulate around damaged fibers to confine Bnl distribution and facilitate tracheal recruitment. Disruption of hemocyte-mediated Bnl or ECM delivery impairs tracheal remodelling and compromises muscle recovery after injury. Together, these findings reveal an immune–muscle–vascular communication module that integrates signalling and matrix remodelling to preserve muscle function following acute damage.

Introduction

Effective tissue repair relies on precise communication and coordination across multiple cell types and tissue systems [1]. Disruption of these interactions can impair regeneration and, in severe cases, compromise organismal survival [2]. In mammals, skeletal muscle regeneration depends on a tightly orchestrated collaboration among various cell types, including macrophages, muscle stem cells (MuSCs, also known as satellite cells), and fibro/adipogenic progenitors (FAPs) [3]. Following injury, macrophages signal to MuSCs to regulate their proliferation and differentiation [4], while vascular adaptations support increased metabolic demands and structural remodelling [5]. Nonetheless, the mechanisms that coordinate cellular recruitment and tissue adaptation to muscle injury remain incompletely understood.

Drosophila frequently encounters natural wounding, requiring efficient tissue adaptation mechanisms to maintain function and ensure survival [6]. *Drosophila* has long served as a powerful model for studying myogenesis [7], and more recently, for uncovering principles of adult muscle regeneration [8-12]. While much attention has focused on the role of *Drosophila* MuSCs in regeneration, relatively little is known about how other cell types contribute to muscle adaptation to damage. In particular, the contribution of the immune blood cells-hemocytes-remains largely unexplored. Despite limited hematopoiesis in adults, hemocytes are essential for detecting and responding to bacterial infections [13]. Approximately 85% of adult hemocytes are plasmatocytes, macrophage-like cells that are distributed throughout the body [14]. Studies, including our own, have shown that they can populate the indirect flight muscles (IFMs) under normal conditions [13,15]. However, whether these immune cells engage in active intercellular signalling following muscle damage, and how they coordinate with other cell types, remains an open question.

The *Drosophila* tracheal cells -a network of air-filled tubes that functions analogously to the vertebrate vascular and respiratory systems- enwrap and penetrate muscle fibers to oxygenate them [16]. These connections are established during development through the FGF/FGFR pathway [17]. The *Drosophila* FGF-like ligand Branchless (Bnl), produced by muscle cells, directs tracheal migration by activating the Breathless (Btl)

receptor on tracheal cells. For decades, tracheal branching has been well characterized at the morphological, cellular, and genetic levels during *Drosophila* development [18-21]. More recently, it has been shown that the adult trachea also undergoes dynamic remodelling to sustain adult gut regeneration [22,23], raising the possibility that similar remodelling could contribute to muscle responses following injury. Hemocytes closely associate with adult trachea [13] suggesting potential cross-talk, but whether hemocytes and tracheal cells cooperate following muscle injury remains unknown.

Here, we report that intercellular communication between muscles, hemocytes, and tracheal cells is coordinated in responses to adult muscle injury. We show that muscle damage triggers rapid and sustained hemocyte recruitment. Hemocyte recruitment is required for targeted tracheal remodelling through Bnl/Btl signalling, enabling selective recognition and support of damaged fibers. In parallel, hemocytes deposit extracellular matrix (ECM) components, including Collagen IV, around injured fibers to spatially confine Bnl and promote tracheal recruitment. Disrupting either tracheal recruitment or hemocyte-mediated ECM delivery impairs muscle performance after injury. These defects underscore the essential roles of both processes in functional recovery. Together, these findings reveal an immune–muscle–vascular signalling module that integrates metabolic support with ECM organization to preserve muscle function after damage.

Results

Hemocytes are recruited to the injured adult flight muscle

Although *Drosophila* is one established model organism for studying muscle repair, it lacks molecular markers that reliably and specifically identify injured muscle fibers. In vertebrates, re-expression of embryonic Myosin Heavy Chain (MyHC-emb) in damaged fibers is a common marker of muscle injury and regeneration [24]. To assess whether Myosin Heavy Chain (Mhc) expression could similarly serve as an indicator of muscle damage in *Drosophila*, we analysed its expression following injury. Our results show that Mhc expression is drastically upregulated in injured muscles (Figure 1 A-F) and inversely correlated with the downregulation of Mef2, providing a robust molecular readout of muscle damage (Figure S1 A-B''). This upregulation persists for at least 20 days post-injury (DPI) (Figure S2 C-L). In *Drosophila*, several Mhc isoforms are generated via alternative splicing of a single *Mhc* gene [25]. To determine which isoform respond to injury, we analysed the expression of various GFP-tagged Mhc isoforms [25,26]. Only the shorter adult Mhc isoforms-K, L, and M-were upregulated in response to muscle damage (Figure S1 C-E''). To rule out the possibility that Mhc upregulation is an artifact of the injury method used, we examined its expression in *Naa30A* mutants, which exhibit developmental defects in flight muscles and spontaneous muscle detachment in eight-day-old adults, along with loss of nuclear Mef2 expression [27]. In these mutants, Mhc upregulation coincided with Mef2 downregulation (Figure S1 F-G''), further supporting Mhc as a reliable marker of muscle damage in *Drosophila*.

To study the hemocytes response to IFMs damage, we started by tracking these cells at various time points after injury using the hemocytes reporters Peroxidasin (*Pxn*) (Figure 1 A-C'') and Hemolectin (*Hml*) (Figure S1 H-I''). Co staining for these markers and Mhc revealed extensive recruitment of hemocytes to the injured muscle fibers (Figure 1 A-C'; Figure S1 H-I''). Notably, while Pxn+ hemocytes persist at the injured muscle for at least 5 DPI, Hml+ hemocytes enrichment declines over time (Figure 1 G), highlighting the heterogeneity of the adult hemocyte population, consistent with previous findings [14]. To further characterize the hemocytes recruitment dynamics, we examined the zinc finger homeodomain transcription factor Zfh1 reporter (*Enh3-Gal4 > UAS-mCD8GFP*), another hemocytes marker [15,28] (Figure 1 D-F''). Enh3+ hemocytes

123 exhibited recruitment kinetics similar to Pxn+ cells (Figure 1 G). Importantly, at 5 DPI
124 all Pxn+ cells were also Enh3+, whereas only a subset of Pxn+ cells were Hml+ (Figure
125 1 G' and Figure S1 H-K'''). None of the recruited Enh3+ hemocytes expressed Mef2
126 (Figure S1 L'-M'). To confirm that hemocytes recruitment is a response to muscle
127 damage, we analyzed *Naa30A* mutants. Consistently, we observed a selective
128 recruitment of Enh3+ hemocytes to injured muscle fibers, identified by high Mhc
129 expression and the loss of Mef2 nuclear expression (Figure 1 H-I'''). Altogether, these
130 data show that adult hemocytes are rapidly and specifically recruited to injured muscle
131 fibers, with distinct subpopulations displaying differential persistence over time.
132

133 **Hemocytes recruitment coordinates with tracheal remodelling following muscle**
134 **injury**

135 The selective recruitment of hemocytes to damaged fibers suggests a role in the
136 muscle damage response. We observed that hemocytes within the IFMs are closely
137 associated with tracheal cells (Figure 2 A-A'). It has previously been shown that
138 tracheal cells can extend new branches toward damaged regions to support adult gut
139 regeneration [22,23]. We therefore asked whether tracheal remodelling also occurs in
140 response to IFMs injury and whether it could be linked to hemocyte recruitment. Our
141 analysis revealed that muscle damage, whether caused by physical injury or in
142 *Naa30A* mutant animals, leads to a significant increase in tracheal coverage of the
143 injured fiber (Figure 2 B-D and Figure S2 A-B'). The invasion is directed toward the
144 injury site, with the highest branching density close to the damaged area and
145 progressively decreasing with distance from the injury (Figure 2 E). We further
146 observed that hemocytes remain spatially close to the tracheal branches, even under
147 injured conditions (Figure 2 C'').

148 To further investigate the tracheal response to injury, we focused on terminal tracheal
149 cells (TTCs), specialized branches of the tracheal system known for their structural
150 plasticity and ability to invade tissues, including muscle fibers, to deliver oxygen [16-18].
151 TTCs can be reliably identified by their distinctive morphology and the expression of
152 the transcription factor Serum Response Factor (dSRF) (Figure 2 F-F' and J-J'). We
153 visualized TTCs by expressing membrane-bound GFP under the control of dSRF-Gal4
154 (*dSRF-Gal4 > UAS-mCD8GFP*) (Figure 2 G-H'''). We observed a high density of TTCs

155 within injured muscle fibers, with the highest concentration near the injury site (Figure
156 2 H-H''' and I). Orthogonal views showed that the recruited trachea are found not only
157 on the muscle surface but also extend branches into the injured fibers (Figure 2 G'''-
158 H'''), consistent with the atypical muscle-tracheal organization optimized to deliver
159 oxygen deep within the muscle, directly to sites of high metabolic demand [16,17].
160 Labelling TTCs nuclei with anti-dSRF confirmed the significant enrichment of dSRF+
161 nuclei along the injured fibers comparing to the uninjured muscles (Figure 2 K-L'' and
162 M). The tracheal enrichment at the injured muscle results from TTCs branching and
163 recruitment rather than proliferation, as no PH3+ cells were detected in the muscle
164 trachea cells (Figure 2 K'''-L'''). Altogether, these data indicate that tracheal cells
165 respond to muscle injury and target specifically the damaged fiber.

166 We found that tracheal enrichment around injured muscles persists throughout the
167 repair process and is still present 20 days post-injury (Figure S2 C-K' and N), a stage
168 at which muscle healing is expected to be complete [9,11]. A comparison of hemocyte
169 recruitment kinetics with tracheal coverage density revealed that hemocyte recruitment
170 precedes tracheal coverage of the injured fibers (Figure S2 M and N), raising the
171 possibility of an interplay between the two-cell population in supporting the injured
172 muscle fiber.

173 **Tracheal invasion of injured muscle fibers is triggered by local hypoxia**

174

175 The tracheal recruitment to injured muscle fibers (Figure 2) suggests a critical oxygen
176 demand of the damaged muscle. If this is the case, local hypoxia within injured fibers
177 could serve as a key cue for tracheal attraction and directional growth toward the site
178 of injury, as seen in other physiological contexts [29]. To assess oxygen variations within
179 the injured muscle, we first used the Synthetic HRE (Hypoxia response element)
180 nuclear sensor (SyHREns), a hypoxia reporter that serves as a proxy for evaluating
181 intracellular oxygen fluctuations [30]. In normal condition, the SyHREns was found to be
182 expressed in some TTCs, identifiable by both their triangular shape and expression of
183 dSRF (Figure 3 A-A''). Importantly, we observed a pronounced enrichment of
184 SyHREns-positive cells surrounding injured muscle fibers, in close proximity to the
185 recruited tracheal branches (Figure 3 B-D''). The high number of SyHREns+ cells
186 around the injured fibers remained stable for at least 20 DPI (Figure 3 E), indicating

187 that local hypoxia persists in parallel with the sustained tracheal remodelling observed
188 over the same period.
189 Hypoxia-induced tracheogenesis is controlled by the transcription factor Similar (Sima)
190 -the *Drosophila* homolog of hypoxia-inducible factor-1α (HIF-1α)- a central regulator of
191 hypoxic and angiogenic responses [29]. Accordingly, silencing *sima* in TTCs severely
192 decreased tracheal expansion towards the injured fibers (Figure 3 F-I). Bnl is a well-
193 established downstream effector of hypoxic signalling, deposited locally on hypoxic
194 tissues to promote tracheal attraction [29]. We therefore hypothesised that if the injured
195 muscle undergoes hypoxia, Bnl should accumulate locally at the damaged fiber to
196 facilitate tracheal remodelling. Analysing the expression of an endogenously tagged
197 *Bnl::GFP*^{endo} allele [31] revealed marked enrichment of Bnl at injured muscle fibers
198 compared to adjacent intact ones (Figure 3 J-K''' and L). Altogether, these data suggest
199 that muscle damage induces local muscle oxygen starvation, which in turn drives
200 tracheal cell recruitment to the injured tissue.

201 **Hemocytes deposit FGF-like ligand Bnl at injured muscles to mediate tracheal**
202 **recruitment**

203 During both embryonic and post-embryonic stages, tracheal guidance is regulated in
204 a dose-dependent manner by local Bnl concentrations [29]. In adult flight muscle
205 development, muscle-tracheal connections are established through the action of Bnl,
206 which is secreted by muscle fibers and acts in a paracrine manner by binding to its
207 receptor, FGFR/Breathless (Btl), expressed on tracheal cells [17]. The observed
208 enrichment of Bnl in injured muscles (Figure 3 J-L) raises two key questions: Is Bnl/Btl
209 signaling functionally involved in directing tracheal recruitment to damaged fibers? If
210 so, what is the source of Bnl enrichment on the injured fibers? To begin addressing
211 these questions, we conditionally overexpressed Bnl in a restricted subset of adult
212 muscle fibers using the flip-out system combined with a regionally expressed driver
213 (Figure S3 A-C and Materials and Methods section). This targeted overexpression was
214 sufficient to recruit tracheal cells to the ectopic Bnl-expressing regions (Figure 4 A-C'),
215 and the extent of this recruitment depended on the duration of Bnl expression:
216 prolonged expression (5 days) triggered more extensive tracheal remodelling than
217 short-term expression (24 hours). These findings showed that the adult tracheal
218 system remains responsive to elevated Bnl levels in the IFMs, supporting the

219 hypothesis that Bnl/Btl signalling directs tracheal pathfinding in response to muscle
220 injury.

221 We next sought to identify the cellular source responsible for Bnl accumulation in
222 injured muscle fibers. Under wild-type conditions, Bnl::GFP^{endo} signal was detected in
223 hemocytes, tracheal cells, and indirect flight muscles (IFMs) (Figure S3 D-D').
224 However, since Bnl is a diffusible protein, these observations alone cannot distinguish
225 between cells that produce Bnl and those that merely take it up. To address this, we
226 used the *Bnl-lacZ* transcriptional reporter, which revealed active *bnl* expression in
227 hemocytes, adult IFMs, and terminal tracheal cells (TTCs), confirming that these cell
228 types are bona fide sources of Bnl under normal conditions (Figure S3 E-F'). Given
229 that canonical Bnl/Btl signalling operates in a paracrine manner, injured muscles and
230 hemocytes emerge as the most plausible sources of injury-induced Bnl accumulation.
231 To distinguish between these two possibilities, we examined *Bnl-lacZ* expression
232 following injury. Surprisingly, we found that injured fibers lacked *Bnl-lacZ* activity,
233 whereas neighboring uninjured fibers retained its expression (Figure 4 D-E''). These
234 findings indicate that the injured muscle fibers themselves do not contribute to the
235 localized Bnl accumulation after injury and suggest that the source of Bnl is extrinsic
236 to the damaged tissue.

237 By contrast, we observed a marked enrichment of Bnl::GFP^{endo} signal surrounding
238 Pxn+ hemocytes recruited to the damaged fibers, suggesting that hemocytes are
239 responsible for depositing Bnl along injured muscles (Figure 4 F-G''). To assess the
240 functional contribution of hemocyte-derived Bnl to tracheal invasion, we selectively
241 silenced *bnl* in hemocytes using either the *Enh3-Gal4* or *HmlΔ-Gal4* drivers. While
242 hemocyte recruitment to injured muscles was unaffected, *bnl* knockdown significantly
243 reduced tracheal invasion into damaged fibers compared with controls (Figure 4 H-J''
244 and K; Figure S3 G-I'' and J). This signalling logic between the two cell types aligns
245 with their close anatomical association under homeostatic conditions (Figure 2 A-A'
246 and [13]).

247 Given the critical role of the tracheal system in supporting tissue function [21], we next
248 asked whether hemocyte-mediated tracheal recruitment via Bnl is required to maintain
249 muscle flight performance after injury. To test this, we performed flight assays on
250 uninjured controls, injured flies, and injured flies in which *bnl* was specifically depleted

from hemocytes. Injured flies exhibited reduced flight capability compared with uninjured controls (Figure 4 L-L'). Importantly, flies lacking hemocyte-derived Bnl showed an even greater impairment in flight, underscoring the functional importance of this signalling in promoting tracheal remodelling and preserving muscle performance following injury (Figure 4 M).

The receptor FGFR/Btl is essential for injury-induced tracheal guided outgrowth

The finding that Bnl orchestrates tracheal morphogenesis in response to muscle damage suggested in turn that it activates its receptor Btl, on tracheal cells, thereby driving guided outgrowth and branching. To investigate this, we examined Btl expression in adult flight muscles using an endogenously tagged *Btl::cherry^{endo}* allele, which faithfully reports Btl expression [31]. Btl::cherry^{endo} was detected along tracheal branches under homeostatic conditions and within tracheal structures invading the injured muscle (Figure 5 A-B''). To complement this approach, we expressed a membrane-tethered GFP (mCD8-GFP) under the control of a *Btl-Gal4* driver (Figure 5 C-E'). While Btl::cherry^{endo} reflects consistent endogenous expression, *Btl-Gal4* drives a more heterogeneous pattern across tracheal cells (Figure 5 C-C'). Nevertheless, we observed a striking accumulation of tracheal branches labelled by *Btl-Gal4* at injured muscles, reinforcing that Btl-expressing tracheal cells are actively recruited to damaged fibers (Figure 5 D-E'). We then tested whether Btl function is required for proper tracheal pathfinding. To this end, *btl* was specifically silenced in tracheal cells using either *dSRF-Gal4* or *Btl-Gal4* drivers (Figure 5 F-I''). In both cases, tracheal invasion into injured fibers was significantly impaired compared to the control (Figure 5 J). Notably, the impairment was more pronounced with *dSRF-Gal4*, consistent with its more uniform expression in terminal tracheal cells (Figure 2 F-F') compared with *Btl-Gal4* (Figure 5 C-C'). Together, these findings show that the Bnl/Btl signalling axis plays a pivotal role in guiding tracheal remodelling after muscle damage. While Btl expression is restricted to tracheal cells, localized Bnl secretion from hemocytes at the damaged fiber refines tracheal pathfinding, ensuring precise and targeted tracheal invasion into injured muscle (Figure 5 K).

282 **Hemocyte-derived ECM retaines Bnl ligand at injured muscles**

283 Although Bnl is a diffusible molecule, we observed that it is specifically retained at the
284 injured fiber (Figure 3 K'-K''), raising the question of what restricts its spatial
285 distribution. Previous studies have shown that Collagen IV, a principal structural
286 component of the muscle ECM, is critical for retaining diffusible signals within defined
287 tissue regions [32]. We therefore hypothesized that ECM components may similarly act
288 to confine Bnl to the damaged fiber.

289 Hemocytes are known to be major producers of ECM components during both
290 *Drosophila* development and post-developmental stages [33,34], suggesting they could
291 supply Collagen IV in response to adult muscle injury. To test this, we analysed
292 Collagen IV distribution in adult flight muscles using the Vkg::GFP line (Figure 6 A-B'').
293 Under homeostatic conditions, we observed a basal level of Vkg::GFP surrounding
294 muscle fibers and along tracheal branches (Figure 6 A'), and we found that hemocytes
295 express Collagen IV (Figure 6 A''). Five days after injury, Vkg::GFP was markedly
296 enriched in damaged fibers compared with intact muscles and uninjured controls
297 (Figure 6 A-B and A''-B''). To further assess the relationship between hemocytes and
298 ECM remodeling, we examined Collagen IV distribution across multiple time points
299 post-injury (1-20 DPI) and compared this to hemocyte recruitment dynamics (Figure 6
300 C-D'' and Figure S4 A-F). Collagen IV accumulation closely correlated with the
301 presence and distribution of hemocytes. Notably, regions where hemocytes were
302 evenly distributed along the injured fiber displayed stronger and more uniform
303 Vkg::GFP signal.

304 To test whether hemocyte-supplied Collagen IV is necessary for Bnl retention at injured
305 fibers, we knocked down Collagen IV specifically in hemocytes and assessed
306 Bnl::GFP^{endo} localization (Figure 6 E-F''). In control flies, Bnl signal was strongly
307 enriched along the injured fiber; however, this enrichment was markedly reduced
308 following Collagen IV depletion (Figure 6 E-F'' and G). These data indicate that
309 Collagen IV is required to retain Bnl at the injury site. Together, these findings show
310 that hemocyte-derived Collagen IV acts as a structural scaffold that immobilizes Bnl at
311 damaged fibers (Figure 6 H). This localized Bnl/Btl signalling likely guides tracheal
312 remodelling and contributes to the maintenance of flight ability.

313 **Hemocyte-derived SPARC supports Collagen IV deposition, tracheal**
314 **remodleling and muscle recovery**

315 Incorporation of Collagen IV into the extracellular matrix (ECM) requires accessory
316 molecules for proper deposition and stabilization. We therefore investigated whether
317 hemocytes also supply such regulatory components. One key factor is SPARC, a
318 collagen-binding glycoprotein essential for Collagen IV diffusion, stabilization, and
319 incorporation into basement membranes [35,36]. We first examined SPARC localization
320 in hemocytes associated with adult IFMs. Hemocytes, identified using *Enh3-Gal4*
321 driver, were positive for SPARC (Figure 6 I-I'). Importantly, following muscle injury,
322 SPARC levels were elevated along the injured fiber compared with controls, mirroring
323 the distribution of Collagen IV (Figure 6 I-J'). These observations suggest that SPARC
324 is locally produced by hemocytes in adult muscle. To further confirm the cellular origin
325 of SPARC enrichment in injured muscles, we employed the SPARC-Gal4 driver, a
326 Gal4 trap line inserted into the endogenous SPARC locus, to drive membrane-targeted
327 RFP (myr-RFP) expression in flies also carrying a BM40-SPARC-GFP fosmid reporter
328 (Figure 6 K-L'). This dual-reporter approach allowed simultaneous visualization of
329 SPARC (via BM40-SPARC-GFP) and identification of SPARC-producing cells (via
330 SPARC-Gal4 > myr-RFP). In uninjured muscle, BM40-SPARC-GFP and SPARC-
331 Gal4-driven myr-RFP were co-expressed in hemocytes. Following injury, BM40-
332 SPARC-GFP was broadly enriched along the damaged fiber, resembling endogenous
333 SPARC protein, whereas SPARC-Gal4 activity remained restricted to hemocytes and
334 was not detected in muscle nuclei (Figure 6 L-L'). Together, these data demonstrate
335 that recruited hemocytes are the primary source of SPARC at injured muscle fibers.
336 We then tested whether hemocyte-derived SPARC is required for Collagen IV
337 enrichment and tracheal remodelling. Depletion of SPARC specifically in hemocytes
338 was sufficient to prevent both Collagen IV accumulation and tracheal remodelling at
339 the injured fiber (Figure 6 M-N'' and O-P). Finally, to evaluate the functional importance
340 of SPARC in the muscle repair process, we performed flight assays and found that
341 injured flies lacking hemocyte-derived SPARC exhibited significantly reduced flight
342 ability compared with controls (Figure 6 Q). Altogether, these results show that
343 hemocyte-derived SPARC is essential for ECM assembly, tracheal remodelling, and
344 functional recovery following muscle injury. They also highlight that hemocytes act as

345 multifunctional signalling hubs, simultaneously delivering trophic, structural, and
346 guidance cues required to coordinate efficient muscle repair.

347 Discussion

348 Our study provides a compelling example of how the muscle damage response relies
349 on the precise coordination between multiple cell types. While *Drosophila* hemocytes
350 are traditionally recognized for their immunoprotective roles against pathogens and
351 infections [13,33,37], our findings reveal that they also play essential roles for repairing
352 injured muscles. We show that hemocytes both signal to the tracheal system to finely
353 regulate its outgrowth toward the injured muscle and directly supply key extracellular
354 matrix (ECM) components to the damaged fiber, two processes that support muscle
355 structural maintenance and recovery post injury (Figure 7).

356 *A functional cooperation between immune cells and the respiratory system*

357 Insect respiration has traditionally been viewed as entirely dependent on the tracheal
358 system, that operates independently of blood cells. However, this view has been
359 challenged by recent finding showing that a subtype of larval hemocytes, known as
360 crystal cells, can take up oxygen from tracheal cells and contribute to tissue
361 oxygenation [38]. Here, we reveal that in adult Drosophila, hemocytes are positioned in
362 close proximity to tracheal cells within muscle tissue and indirectly contribute to oxygen
363 delivery by guiding tracheal branches toward sites of muscle injury (Figure 7).
364 Following damage, hemocytes are rapidly recruited to and spread over the injured
365 muscle surface. They secrete Bnl that promote local tracheal outgrowth and precise
366 branch targeting. This finding raises an intriguing question: Why does the injured
367 muscle, the structure directly damaged, not itself produce Bnl? Put differently, why
368 delegate to extrinsic immune cells the ability to attract tracheal branches when the
369 demand for oxygen and repair arises intrinsically within the muscle? One possible
370 explanation lies in the need to prevent inappropriate or excessive activation of tracheal
371 growth programs. Bnl is a potent chemoattractant, and its widespread expression
372 within muscle fibers could trigger aberrant tracheogenesis, leading to the recruitment
373 of non-specific tracheal branches and disruption of the normal tracheal network
374 architecture. Hemocytes, by contrast, are far less numerous than muscle fiber nuclei
375 and, once localized along the damaged area, could secrete limited amounts of Bnl in

376 a spatially restricted manner. Such targeted release would ensure that tracheal
377 outgrowth occurs only at sites where oxygen delivery and tissue repair are most
378 needed.

379 Beyond their indirect role in oxygenation, which is mediated through the guidance of
380 the tracheal network, it remains to be determined whether adult hemocytes might also
381 directly contribute to oxygen transport, as has been described with crystal cells during
382 larval stages [38]. Interestingly, during development, some plasmatocytes have been
383 shown to transdifferentiate into crystal cells in the lymph gland, the primary
384 hematopoietic organ [39]. Whether a similar transdifferentiation occurs in the adult
385 following muscle injury remains an open question. The nature of the signals that govern
386 hemocyte recruitment under injury conditions remains an important avenue for future
387 investigation.

388 ***Do Drosophila repair or regenerate their flight muscles?***

389 The IFMs generate the high-frequency wing beats that enable flight, a behavior
390 essential for predator avoidance, foraging, and mating. Given their vital function, IFMs
391 must be maintained in optimal condition to ensure sustained performance throughout
392 the animal's lifespan. This need for resilience is also underscored by the observation
393 that over 30% of wild-caught *Drosophila* exhibit physical injuries, frequently located in
394 the thorax and abdomen [6]. Although a rare population of satellite-like cells has been
395 identified in adult flies, the regenerative capacity of adult *Drosophila* muscles remains
396 debated [40]. A major limitation has been the lack of appropriate molecular markers to
397 monitor both muscle regeneration and muscle stem cell (MuSC) activity. In our study,
398 we identified a specific isoform of the Myosin Heavy Chain (Mhc) that is consistently
399 upregulated in damaged fibers. However, unlike in vertebrates, where MyHC-emb
400 levels return to baseline following regeneration, Mhc expression in *Drosophila* remains
401 elevated even 20 days post-injury (Figure S2). This makes Mhc a sensitive marker for
402 identifying injury, but less useful for assessing complete muscle recovery. Adult MuSCs
403 have been identified via the transcription factor Zfh1/ZEB and its reporter Enh3 [11,15],
404 the only presently known marker for these cells. Zfh1 is required for MuSCs
405 maintenance, an equivalent role of ZEB was subsequently shown in mice [41].
406 Interestingly, both Zfh1 and ZEB are expressed in the muscle associated immune cells
407 [15,41]. In our study, we found that following muscle injury, 100% of the cells recruited to

damaged fibers are both Enh3$^+$ and Pxn$^+$ (a plasmatocytes marker), while being negative for the muscle-specific marker Mef2 (Figure S1 L-M'). This strongly suggests that hemocytes are the predominant, if not exclusive cell population migrating to injured muscle. These findings suggest that adult *Drosophila* flight muscles possess limited intrinsic regenerative capacity and may instead rely on compensatory mechanisms such as increased oxygenation through tracheal remodelling and structural reinforcement via extracellular matrix (ECM) deposition-to cope with muscle damage. This is consistent with the broader idea that short-lived species prioritize immediate survival over long-term regenerative investment [42]. In such organisms, evolution favors fast and efficient repair mechanisms that support rapid recovery and fitness over complex, energy-intensive regeneration programs.

Functional parallels between Drosophila hemocytes and mammalian FAPs

In mammals, extracellular matrix (ECM) remodeling is essential for maintaining muscle structure and enabling proper tissue repair. Although muscle stem cells (MuSCs) can produce some ECM components [43], the primary contributors to ECM production and maintenance during regeneration are fibro-adipogenic progenitors (FAPs) [44]. *Drosophila* lack dedicated FAPs, raising the question of how flies achieve ECM remodelling and maintain muscle integrity. During development, hemocytes are the primary source of ECM molecule production [33,45,46]. However, functional evidence for their involvement in ECM remodeling in adult tissues-particularly muscle-has remained limited. Here, we showed that adult hemocytes produce at least two key ECM components -Collagen IV and SPARC. This production is particularly enriched around damaged muscle fibers where hemocytes are abundant. We further showed that hemocyte-specific ablation of ECM led to defect in muscle post injury recovery. These findings suggest that *Drosophila* hemocytes share functional similarities with mammalian FAPs and may compensate for their absence. This highlights an evolutionarily flexible strategy for achieving muscle repair in organisms with fewer specialized cell types.

440 ## Materials and Methods

441 ### *Drosophila melanogater* strains and genetics

442 All *Drosophila melanogaster* stocks were grown on standard medium at 25°C. The
443 following stains were used: *w*^{118} as wild type (wt), *Pxn-RFP* [47], *HmlΔ-Gal4* (BL#30140),
444 *Enh3-Gal4* [15], *Mhc-Iso-K, L, M (fTRG500)* and *Mhc-Iso-A, F, G (fTRG519)* [26], *weeP26*
445 [25], *Bnl::GFP*^{endo} *and Btl::cherry*^{endo} [31], *Bnl-LacZ* (BL#11704), , *dSRF-GAL4* (BL#25753),
446 *Btl-Gal4* (BL#78328), *UAS-Btl*^{RNAi} (BL#435544), *UAS-Bnl*^{RNAi} (BL#34572), *UAS-*
447 *Bnl::GFP* [48], *Vkg::GFP* (BL#98343), *BM40-SPARC-GFP* (Sarov et al., 2016), *SME-*
448 *Gal4* (VT 0576871), *UAS-H2B-RFP* [49], *UAS-mCD8GFP* (BL#5137), *UAS-myr-mRFP*
449 (BL#7118), SyHREns [30], *UAS-Sima*^{RNAi} (BL#26207), *SPARC-Gal4* (BL#77473), *UAS-*
450 *SPARC*^{RNAi} (BL#40885), *UAS-Vkg*^{RNAi} (BL#50895). *Naa30A* deletion males were
451 obtained from crosses between *Naa30A*$^{\Delta 74}$*/FM0* females and either UAS-mCD8GFP;
452 Enh3-Gal4 (Figure 1) or Mhc-Iso-K, L, M (Figure S1) males. RNAi experiments were
453 carried out at 29°C. To achieve temporal control of gene expression in adult tissues,
454 the tubGal80^{ts} was employed, allowing restriction of Gal4 activity to a specific time
455 window. Fly crosses were initially maintained at 18°C, and after adult eclosion, the
456 progenies were transferred to 29°C, where they remained until dissection. An
457 exception was made for the Bnl knockdown experiments shown in Figure 4 J-J'', which
458 were performed without the tubGal80^{ts} transgene.
459

460 **Generation of SME-FRT-stop-FRT-Gal4 fly line and flip-out induction procedure.**

461 SME (Shavenbaby Muscle Enhancer) is one of several enhancers of the *shavenbaby*
462 gene (VT057071-Gal4). It is active in larval muscle progenitors (AMPs) (Figure S3 A-
463 A') and remains active in a subpopulation of localized muscle nuclei in the adult indirect
464 flight muscles (IFMs) (Figure S3 B-B'). To generate the SME-FRT-stop-FRT-Gal4
465 construct, the cis-regulatory element from the original *shavenbaby* enhancer construct
466 was used to replace the *pAct* promoter in the pAct-FRT-stop-FRT3-FRT-FRT3-Gal4
467 vector (Addgene plasmid #52889). The resulting construct was integrated into the attP
468 site at cytological location 51D on chromosome II via embryo injection into vas-int; attP-
469 51D flies. To induce localized overexpression of Bnl::GFP in adult IFM nuclei, hsflp;
470 FRT-SME-stop-FRT-Gal4/CyO; tubGal80^{ts} females were crossed to UAS-Bnl::GFP

471 males. Progeny were raised at 18°C and subjected to a 2-hour heat shock at 37°C in
472 young adulthood (Figure 4 A-C').

473 **Immunohistochemistry and confocal microscopy**
474
475 Preparation and immunofluorescence of wing discs and adult muscles were performed
476 as previously described in [50]. The following primary antibody were used: Chicken anti-
477 βGal (1:100, Abcam, ab9361), Chicken anti-GFP (1:300, Abcam, ab13970), Mouse
478 anti-Mhc (1:200, DSHB, 3E8-3D3-s) , Mouse anti-dSRF (1:20, a gift from Mark A.
479 Krasnow, Stanford university California , USA), Rabbit anti-Mef2 (1:500 , DSHB, Mef2-
480 p), Rabbit anti-PH3 (1:100, Cell Signaling Technology, #9713), Rabbit anti-SPARC
481 (1:500, a gift from Maurice Ringuette, University of Toronto, Canada), Rat anti-RFP
482 (1:800, Chromotek, 5F8-20), Alexa-conjugated Phalloidin (1:200, Thermo fisher
483 scientific life technologies).
484
485 **Induction of flight muscle injury**
486
487 Flight muscle injury was induced following previously described protocol [51]. Adult flies
488 (2-3 days post-eclosion) were anesthetized and positioned laterally under a
489 stereomicroscope. A single, localized stab wound was inflicted manually using a fine
490 stainless-steel needle (Minutien Pins, 0.1 mm diameter; #26002–10) to minimize tissue
491 damage and avoid extensive injury. Age-matched, uninjured flies served as controls.
492
493 **Flight assay**

494 Flight ability was assessed using a 1-m-long cylindrical flight column internally lined
495 with paper coated with a thin layer of glue. The adhesive sheet was divided evenly into
496 three longitudinal sections corresponding to the Top**,** Middle, and Bottom regions of
497 the tube (Figure 4L). For each experimental condition, an equal number of flies
498 (approximately 20–30) was released into the tube. After all flies had landed, the paper
499 was removed, flattened, and imaged for analysis.

500 Image quantification was performed semi-automatically using a custom R script, Fly-
501 Spy (available at https://github.com/Olivier-Josse/Fly-spy). Images were first
502 converted to grayscale and digitally divided into the three predefined regions. High-

503 intensity spots corresponding to individual flies were identified by applying a manually
504 adjusted threshold to ensure accurate segmentation. The number of flies detected in
505 each region was quantified and expressed as a percentage of the total recovered flies.
506 The distribution of flies across the three regions—reflecting high, intermediate, or
507 low/absent flight ability—was compared between experimental conditions using a chi-
508 square (χ^2) test. Results are presented as stacked bar histograms

509 **Microscopy and data analysis**

510 Samples were imaged using a Leica SP8 microscope (BIOSIT, University of Rennes)
511 at 20×, 40×, or 63× magnification and a resolution of 1024×1024 pixels. Images were
512 processed with ImageJ and assembled using Adobe Illustrator. To quantify
513 fluorescence intensity, all samples were processed and analyzed in parallel under
514 identical conditions. Confocal images were acquired using the same laser settings
515 across all samples. Sum slice projections were generated from each confocal stack.
516 Regions of interest (ROIs) were manually defined based on protein expression, and
517 mean fluorescence intensities were measured within each ROI. These values were
518 then normalized to background levels measured in comparable areas of the same
519 sample.

520 Tracheal branches were visualized either by their intrinsic autofluorescence using a
521 405 nm UV laser [16] or by the expression of membrane-bound GFP driven by a tracheal-
522 specific Gal4 driver (UAS-mCD8GFP). Tracheal coverage was quantified as pixel area
523 per muscle fiber from maximum intensity Z-projections acquired at 20× magnification.
524 Quantification was performed using the “Skeletonize” plugin in ImageJ, based on the
525 method described by Perochon et al. (2021) [23], with minor modifications. Briefly,
526 maximum intensity projections were generated from each confocal stack, tracheal
527 branches were segmented by thresholding, and the resulting images were
528 skeletonized. Skeleton pixel intensity was then measured specifically within injured
529 muscle fibers and their corresponding contralateral control fibers. For Figure 2E,
530 square regions of interest (ROIs) were placed at the injury site, as well as in proximal
531 and distal regions, to assess local tracheal enrichment. Hemocyte and dSRF-positive
532 cell numbers were quantified manually using ImageJ.

Graphs and statistical analyses were performed using GraphPad Prism. Pair comparisons were statistically tested with a two-sided Student's t-test. NS, not significant ($p>0.05$); *$p < 0.05$, **$p < 0.01$, ***$p < 0.001$ ****$p< 0.0001$.

Acknowledgments

We would like to thank Jennifer Zanet, Cedric Polesello, Sougata Roy, Ruth Lehmann, Maurice Ringuette, Jean-Paul Vincent, and Mark A. Krasnow, as well as the Bloomington Drosophila Stock Center, the Vienna Drosophila Resource Center (VDRC), and the Developmental Studies Hybridoma Bank for providing *Drosophila* strains and antibodies. We are grateful to Lucas Waltzer, Laetitia Bataille, Alain Vincent, and Michèle Crozatier for their critical reading of the manuscript, and to other members of H.B's laboratory for valuable discussions. We also thank Emmanuel Gallaud for helpful input during the early phases of the project. We acknowledge Xavier Pinson from the Microscopy Rennes Imaging Center (MRic, BIOSIT, Biogenouest) for technical assistance, and Cyrille Surbled for fly stock maintenance and technical help. Work in the Boukhatmi lab was supported by an AFM-Téléthon Trampoline Grant (#23108), ATIP-Avenir (CNRS), and ANR GenepiMuSC (ANR-23-CE13-0006). N.A. was supported by an AFM-Téléthon PhD fellowship (#23846) and an FRM fellowship (FDT202404018608). Work in the Cordero lab was supported by a Sir Henry Dale Fellowship (Wellcome Trust and Royal Society, 104103/Z/14/Z), a Wellcome ISSF Returner Scheme (204820/Z/16/Z), and a Tenovus Fellowship (Tenovus/S22-28) to J.P.

Competing interest

The authors declare that they have no competing interests.

567 **Reference**
568

569 1. Sun, F., and Poss, K.D. (2023). Inter-organ communication during tissue regeneration.
570 Development *150*. 10.1242/dev.202166.
571 2. Li, J., Zhang, S., and Amaya, E. (2016). The cellular and molecular mechanisms of
572 tissue repair and regeneration as revealed by studies in Xenopus. Regeneration (Oxf)
573 *3*, 198-208. 10.1002/reg2.69.
574 3. Relaix, F., Bencze, M., Borok, M.J., Der Vartanian, A., Gattazzo, F., Mademtzoglou, D.,
575 Perez-Diaz, S., Prola, A., Reyes-Fernandez, P.C., Rotini, A., and Taglietti, t. (2021).
576 Perspectives on skeletal muscle stem cells. Nature Communications *12*, 692.
577 10.1038/s41467-020-20760-6.
578 4. Dort, J., Fabre, P., Molina, T., and Dumont, N.A. (2019). Macrophages Are Key
579 Regulators of Stem Cells during Skeletal Muscle Regeneration and Diseases. Stem
580 Cells Int *2019*, 4761427. 10.1155/2019/4761427.
581 5. Eming, S.A., Martin, P., and Tomic-Canic, M. (2014). Wound repair and regeneration:
582 mechanisms, signaling, and translation. Sci Transl Med *6*, 265sr266.
583 10.1126/scitranslmed.3009337.
584 6. Subasi, B.S., Grabe, V., Kaltenpoth, M., Rolff, J., and Armitage, S.A.O. (2024). How
585 frequently are insects wounded in the wild? A case study using Drosophila
586 melanogaster. R Soc Open Sci *11*, 240256. 10.1098/rsos.240256.
587 7. Laurichesse, Q., and Soler, C. (2020). Muscle development : a view from adult
588 myogenesis in Drosophila. Semin Cell Dev Biol *104*, 39-50.
589 10.1016/j.semcdb.2020.02.009.
590 8. Gunage, R.D., Dhanyasi, N., Reichert, H., and VijayRaghavan, K. (2017). Drosophila
591 adult muscle development and regeneration. Semin Cell Dev Biol *72*, 56-66.
592 10.1016/j.semcdb.2017.11.017.
593 9. Catalani, E., Zecchini, S., Giovarelli, M., Cherubini, A., Del Quondam, S., Brunetti, K.,
594 Silvestri, F., Roux-Biejat, P., Napoli, A., Casati, S.R., et al. (2022). RACK1 is evolutionary
595 conserved in satellite stem cell activation and adult skeletal muscle regeneration. Cell
596 Death Discovery *8*, 459. 10.1038/s41420-022-01250-8.
597 10. Goh, K.Y., Lee, W.X., Choy, S.M., Priyadarshini, G.K., Chua, K., Tan, Q.H., Low, S.Y., Chin,
598 H.S., Wong, C.S., Huang, S.Y., et al. (2024). FOXO-regulated DEAF1 controls muscle
599 regeneration through autophagy. Autophagy *20*, 2632-2654.
600 10.1080/15548627.2024.2374693.
601 11. Chaturvedi, D., Reichert, H., Gunage, R.D., and VijayRaghavan, K. (2017). Identification
602 and functional characterization of muscle satellite cells in Drosophila. Elife *6*.
603 10.7554/eLife.30107.
604 12. Boukhatmi, H. (2021). Drosophila, an Integrative Model to Study the Features of
605 Muscle Stem Cells in Development and Regeneration. Cells *10*.
606 10.3390/cells10082112.
607 13. Sanchez Bosch, P., Makhijani, K., Herboso, L., Gold, K.S., Baginsky, R., Woodcock, K.J.,
608 Alexander, B., Kukar, K., Corcoran, S., Jacobs, T., et al. (2019). Adult Drosophila Lack
609 Hematopoiesis but Rely on a Blood Cell Reservoir at the Respiratory Epithelia to Relay
610 Infection Signals to Surrounding Tissues. Dev Cell *51*, 787-803 e785.
611 10.1016/j.devcel.2019.10.017.
612 14. Boulet, M., Renaud, Y., Lapraz, F., Benmimoun, B., Vandel, L., and Waltzer, L. (2021).
613 Characterization of the Drosophila Adult Hematopoietic System Reveals a Rare Cell

614 Population With Differentiation and Proliferation Potential. Front Cell Dev Biol *9*,
615 739357. 10.3389/fcell.2021.739357.
616 15. Boukhatmi, H., and Bray, S. (2018). A population of adult satellite-like cells in
617 Drosophila is maintained through a switch in RNA-isoforms. Elife *7*.
618 10.7554/eLife.35954.
619 16. Sauerwald, J., Backer, W., Matzat, T., Schnorrer, F., and Luschnig, S. (2019). Matrix
620 metalloproteinase 1 modulates invasive behavior of tracheal branches during entry
621 into Drosophila flight muscles. Elife *8*. 10.7554/eLife.48857.
622 17. Peterson, S.J., and Krasnow, M.A. (2015). Subcellular trafficking of FGF controls
623 tracheal invasion of Drosophila flight muscle. Cell *160*, 313-323.
624 10.1016/j.cell.2014.11.043.
625 18. Ghabrial, A., Luschnig, S., Metzstein, M.M., and Krasnow, M.A. (2003). Branching
626 morphogenesis of the Drosophila tracheal system. Annu Rev Cell Dev Biol *19*, 623-
627 647. 10.1146/annurev.cellbio.19.031403.160043.
628 19. Rao, P.R., Lin, L., Huang, H., Guha, A., Roy, S., and Kornberg, T.B. (2015).
629 Developmental compartments in the larval trachea of Drosophila. Elife *4*.
630 10.7554/eLife.08666.
631 20. Ebner, A., Kiefer, F.N., Ribeiro, C., Petit, V., Nussbaumer, U., and Affolter, M. (2002).
632 Tracheal development in Drosophila melanogaster as a model system for studying the
633 development of a branched organ. Gene *287*, 55-66. 10.1016/s0378-1119(01)00895-
634 2.
635 21. Hayashi, S., and Kondo, T. (2018). Development and Function of the Drosophila
636 Tracheal System. Genetics *209*, 367-380. 10.1534/genetics.117.300167.
637 22. Tamamouna, V., Rahman, M.M., Petersson, M., Charalambous, I., Kux, K., Mainor, H.,
638 Bolender, V., Isbilir, B., Edgar, B.A., and Pitsouli, C. (2021). Remodelling of oxygen-
639 transporting tracheoles drives intestinal regeneration and tumorigenesis in
640 Drosophila. Nat Cell Biol *23*, 497-510. 10.1038/s41556-021-00674-1.
641 23. Perochon, J., Yu, Y., Aughey, G.N., Medina, A.B., Southall, T.D., and Cordero, J.B.
642 (2021). Dynamic adult tracheal plasticity drives stem cell adaptation to changes in
643 intestinal homeostasis in Drosophila. Nat Cell Biol *23*, 485-496. 10.1038/s41556-021-
644 00676-z.
645 24. Murphy, M.M., Lawson, J.A., Mathew, S.J., Hutcheson, D.A., and Kardon, G. (2011).
646 Satellite cells, connective tissue fibroblasts and their interactions are crucial for
647 muscle regeneration. Development *138*, 3625-3637. 10.1242/dev.064162.
648 25. Orfanos, Z., and Sparrow, J.C. (2013). Myosin isoform switching during assembly of
649 the Drosophila flight muscle thick filament lattice. J Cell Sci *126*, 139-148.
650 10.1242/jcs.110361.
651 26. Sarov, M., Barz, C., Jambor, H., Hein, M.Y., Schmied, C., Suchold, D., Stender, B.,
652 Janosch, S., K, J.V., Krishnan, R.T., et al. (2016). A genome-wide resource for the
653 analysis of protein localisation in Drosophila. Elife *5*, e12068. 10.7554/eLife.12068.
654 27. Varland, S., Silva, R.D., Kjosas, I., Faustino, A., Bogaert, A., Billmann, M., Boukhatmi,
655 H., Kellen, B., Costanzo, M., Drazic, A., et al. (2023). N-terminal acetylation shields
656 proteins from degradation and promotes age-dependent motility and longevity. Nat
657 Commun *14*, 6774. 10.1038/s41467-023-42342-y.
658 28. Wu, W.H., Kuo, T.H., Kao, C.W., Girardot, C., Hung, S.J., Liu, T., Furlong, E.E.M., and Liu,
659 Y.H. (2019). Expanding the mesodermal transcriptional network by genome-wide

660 identification of Zinc finger homeodomain 1 (Zfh1) targets. FEBS Lett *593*, 1698-1710.
661 10.1002/1873-3468.13443.
662 29. Jarecki, J., Johnson, E., and Krasnow, M.A. (1999). Oxygen regulation of airway
663 branching in Drosophila is mediated by branchless FGF. Cell *99*, 211-220.
664 10.1016/s0092-8674(00)81652-9.
665 30. Zhao, Y., Alexandre, C., Kelly, G., Perez-Mockus, G., and Vincent1, J.-P. (2024). Growth-
666 induced physiological hypoxia correlates with growth deceleration during normal
667 development. bioRxiv. https://doi.org/10.1101/2024.06.04.597345.
668 31. Du, L., Sohr, A., Yan, G., and Roy, S. (2018). Feedback regulation of cytoneme-
669 mediated transport shapes a tissue-specific FGF morphogen gradient. Elife *7*.
670 10.7554/eLife.38137.
671 32. Wang, X., Harris, R.E., Bayston, L.J., and Ashe, H.L. (2008). Type IV collagens regulate
672 BMP signalling in Drosophila. Nature *455*, 72-77. 10.1038/nature07214.
673 33. Gold, K.S., and Bruckner, K. (2015). Macrophages and cellular immunity in Drosophila
674 melanogaster. Semin Immunol *27*, 357-368. 10.1016/j.smim.2016.03.010.
675 34. Bunt, S., Hooley, C., Hu, N., Scahill, C., Weavers, H., and Skaer, H. (2010). Hemocyte-
676 secreted type IV collagen enhances BMP signaling to guide renal tubule
677 morphogenesis in Drosophila. Dev Cell *19*, 296-306. 10.1016/j.devcel.2010.07.019.
678 35. Bradshaw, A.D. (2009). The role of SPARC in extracellular matrix assembly. J Cell
679 Commun Signal *3*, 239-246. 10.1007/s12079-009-0062-6.
680 36. Chioran, A., Duncan, S., Catalano, A., Brown, T.J., and Ringuette, M.J. (2017). Collagen
681 IV trafficking: The inside-out and beyond story. Dev Biol *431*, 124-133.
682 10.1016/j.ydbio.2017.09.037.
683 37. Kalra, S., Bahendeka, S., Sahay, R., Ghosh, S., Md, F., Orabi, A., Ramaiya, K., Al
684 Shammari, S., Shrestha, D., Shaikh, K., et al. (2018). Consensus Recommendations on
685 Sulfonylurea and Sulfonylurea Combinations in the Management of Type 2 Diabetes
686 Mellitus - International Task Force. Indian J Endocrinol Metab *22*, 132-157.
687 10.4103/ijem.IJEM_556_17.
688 38. Shin, M., Chang, E., Lee, D., Kim, N., Cho, B., Cha, N., Koranteng, F., Song, J.J., and
689 Shim, J. (2024). Drosophila immune cells transport oxygen through PPO2 protein
690 phase transition. Nature *631*, 350-359. 10.1038/s41586-024-07583-x.
691 39. Marcetteau, J., Duarte, P., Leitao, A.B., and Sucena, E. (2025). Transdifferentiation of
692 plasmatocytes to crystal cells in the lymph gland of Drosophila melanogaster. EMBO
693 Rep *26*, 2077-2097. 10.1038/s44319-025-00366-z.
694 40. Chechenova, M., McLendon, L., Dallas, B., Stratton, H., Kiani, K., Gerberich, E.,
695 Alekseyenko, A., Tamba, N., An, S., Castillo, L., et al. (2024). Muscle degeneration in
696 aging Drosophila flies: the role of mechanical stress. Skelet Muscle *14*, 20.
697 10.1186/s13395-024-00352-4.
698 41. Siles, L., Ninfali, C., Cortes, M., Darling, D.S., and Postigo, A. (2019). ZEB1 protects
699 skeletal muscle from damage and is required for its regeneration. Nature
700 Communications *10*, 1364. 10.1038/s41467-019-08983-8.
701 42. Kirkwood, T.B. (2005). Understanding the odd science of aging. Cell *120*, 437-447.
702 10.1016/j.cell.2005.01.027.
703 43. Baghdadi, M.B., Castel, D., Machado, L., Fukada, S.I., Birk, D.E., Relaix, F., Tajbakhsh,
704 S., and Mourikis, P. (2018). Reciprocal signalling by Notch-Collagen V-CALCR retains
705 muscle stem cells in their niche. Nature *557*, 714-718. 10.1038/s41586-018-0144-9.

44. Molina, T., Fabre, P., and Dumont, N.A. (2021). Fibro-adipogenic progenitors in skeletal muscle homeostasis, regeneration and diseases. Open Biol *11*, 210110. 10.1098/rsob.210110.
45. Shahab, J., Baratta, C., Scuric, B., Godt, D., Venken, K.J., and Ringuette, M.J. (2015). Loss of SPARC dysregulates basal lamina assembly to disrupt larval fat body homeostasis in Drosophila melanogaster. Dev Dyn *244*, 540-552. 10.1002/dvdy.24243.
46. Mase, A., Augsburger, J., and Bruckner, K. (2021). Macrophages and Their Organ Locations Shape Each Other in Development and Homeostasis - A Drosophila Perspective. Front Cell Dev Biol *9*, 630272. 10.3389/fcell.2021.630272.
47. Rodrigues, D., Renaud, Y., VijayRaghavan, K., Waltzer, L., and Inamdar, M.S. (2021). Differential activation of JAK-STAT signaling reveals functional compartmentalization in Drosophila blood progenitors. Elife *10*. 10.7554/eLife.61409.
48. Lin, L. (2009). Clonal Analysis of Growth Behaviors During Drosophila Larval Tracheal Development In Doctoral thesis. (University of Basel).
49. Antonello, Z.A., Reiff, T., Ballesta-Illan, E., and Dominguez, M. (2015). Robust intestinal homeostasis relies on cellular plasticity in enteroblasts mediated by miR-8-Escargot switch. EMBO J *34*, 2025-2041. 10.15252/embj.201591517.
50. Leroux, E., Ammar, N., Moinet, S., Pecot, T., and Boukhatmi, H. (2023). Studying Muscle Transcriptional Dynamics at Single-molecule Scales in Drosophila. J Vis Exp. 10.3791/65713.
51. Chakraborty, K., VijayRaghavan, K., and Gunage, R. (2018). A Method to Injure, Dissect and Image Indirect Flight Muscle of Drosophila. Bio Protoc *8*, e2860. 10.21769/BioProtoc.2860.

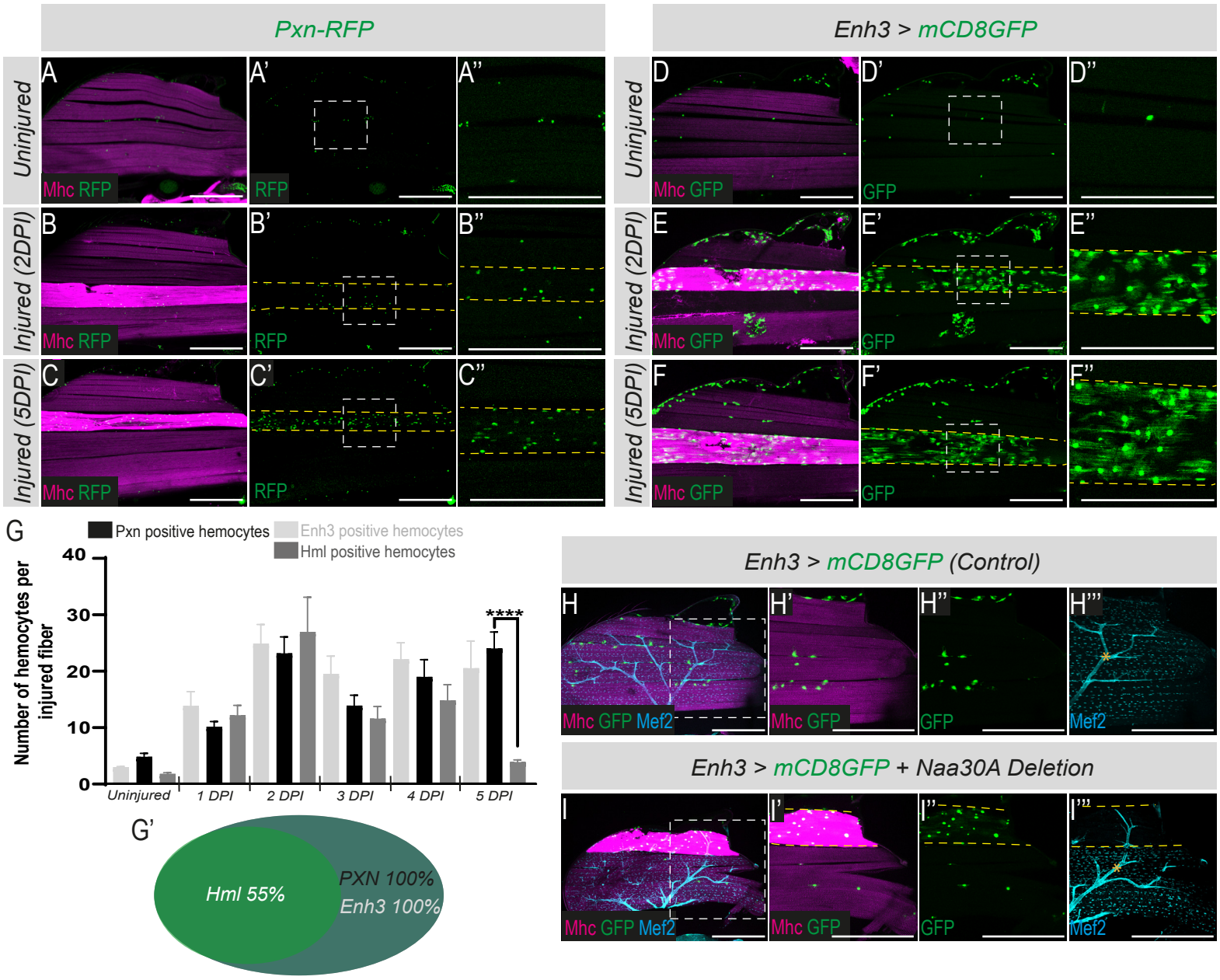
Pxn-RFP
Enh3 > mCD8GFP
Uninjured
Injured (2DPI)
Injured (5DPI)
A
A'
A''
B
B'
B''
C
C'
C''
D
D'
D''
E
E'
E''
F
F'
F''
Mhc RFP
RFP
Mhc GFP
GFP
G
Pxn positive hemocytes
Enh3 positive hemocytes
Hml positive hemocytes
Number of hemocytes per injured fiber
40
30
20
10
0
****
Uninjured
1 DPI
2 DPI
3 DPI
4 DPI
5 DPI
G'
Hml 55%
PXN 100%
Enh3 100%
Enh3 > mCD8GFP (Control)
H
H'
H''
H'''
Mhc GFP Mef2
Mhc GFP
GFP
Mef2
Enh3 > mCD8GFP + Naa30A Deletion
I
I'
I''
I'''

Figure 1

Figure 1. Hemocytes are specifically recruited to the damaged muscle fiber. (A-F). Adult indirect flight muscles (IFMs) imaged under uninjured conditions and at 2-and 5-days post-injury (2DPI and 5DPI). Mhc (magenta) marks muscles. Hemocytes (green) are visualized using the following reporters: *Pxn-RFP* in (A-C'') and *Enh3-Gal4; UAS-mCD8GFP* in (D-F''). Dashed yellow outlines indicate injured muscle fibers showing elevated Mhc expression. **(G)**. Time-course analysis of hemocytes recuitment at 1, 2, 3, 4 and 5 DPI reveals heterogeneous kinetics of response to muscle damage. Enh3-positive, Pxn-positive, and Hml-positive hemocytes are represented by light gray, black, and dark gray bars, respectively (****$p < 0.0001$, Student's t-test; $n \geq 10$ heminota per condition). **(G').** Schematic representation of the proportion of recruited hemocytes expressing different reporters. **(H-I''').** Distribution of hemocytes visualized with *Enh3-Gal4; UAS-mCD8GFP* (green) in control muscles (H-H''') and *Naa30A* mutants (I-I'''). Muscles and muscle nuclei are stained with Mhc (magenta) and Mef2 (cyan) respectively. Scale bar: 200µm. Asterisks in panels H''' and I''' mark non-specific signal detected in motoneurons.

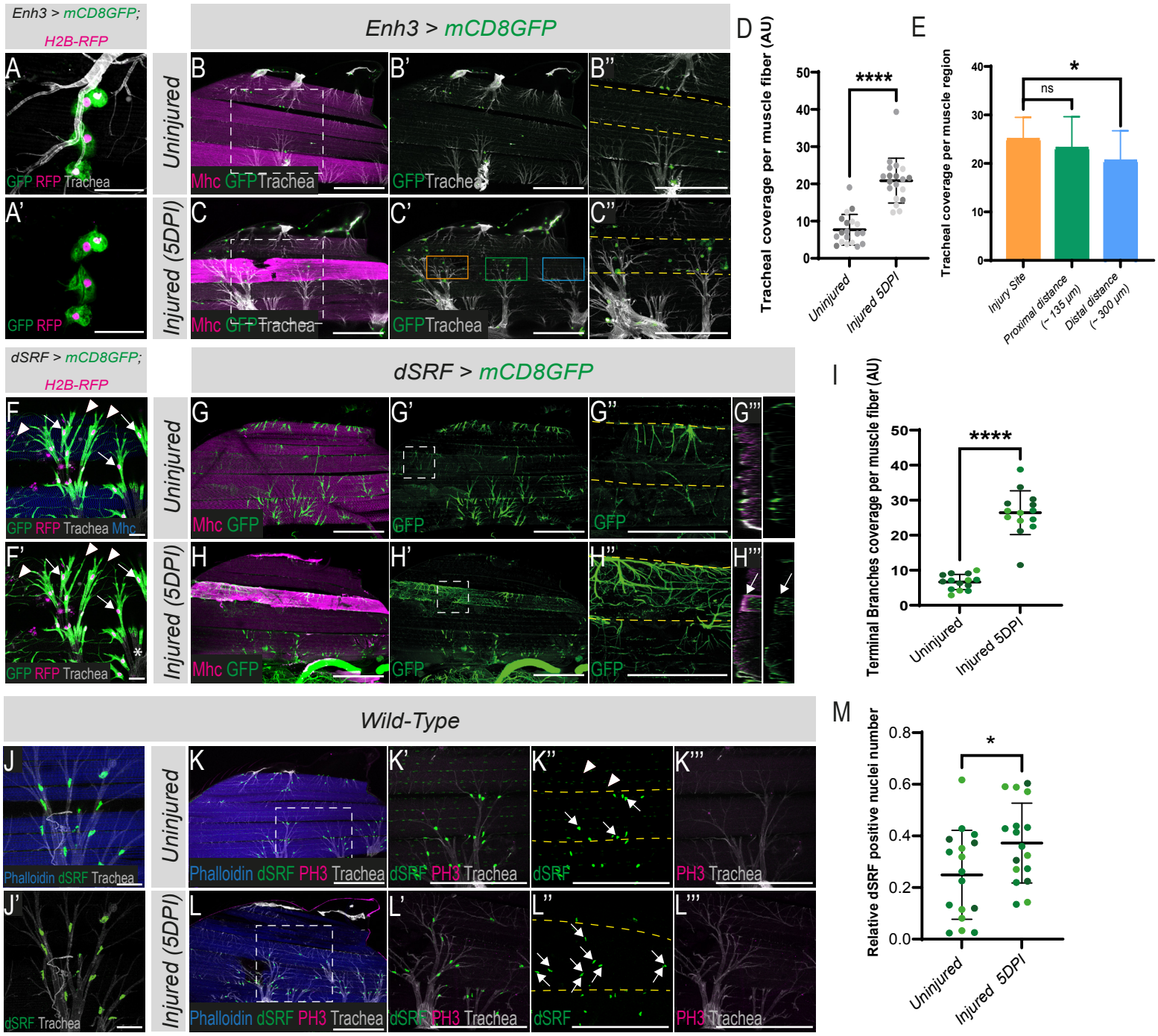
Enh3 > mCD8GFP;
H2B-RFP
Enh3 > mCD8GFP
Uninjured
Injured (5DPI)
GFP RFP Trachea
Mhc GFP Trachea
GFP Trachea
GFP RFP
D
Tracheal coverage per muscle fiber (AU)
****
Uninjured
Injured 5DPI
E
Tracheal coverage per muscle region
ns
*
Injury Site
Proximal distance (~ 135 µm)
Distal distance (~ 300 µm)
dSRF > mCD8GFP;
H2B-RFP
dSRF > mCD8GFP
GFP RFP Trachea Mhc
Mhc GFP
GFP
I
Terminal Branches coverage per muscle fiber (AU)
****
Uninjured
Injured 5DPI
Wild-Type
Phalloidin dSRF Trachea
Phalloidin dSRF PH3 Trachea
dSRF PH3 Trachea
dSRF
PH3 Trachea
dSRF Trachea
M
Relative dSRF positive nuclei number
*
Uninjured
Injured 5DPI

Figure 2

Figure 2. Muscle damage induces directed tracheal remodelling. (A-A'). Hemocytes (green/magenta; *Enh3-Gal4, UAS-mCD8GFP; UAS-H2B-RFP*) are associated to the muscle tracheal cells (gray, autofluorescence). Scale bars: 25 µm. **(B-C'').** Distribution of tracheal branches (gray, autofluorescence) and hemocytes (green, *Enh3-Gal4; UAS-mCD8GFP*) in control (B-B'') and at 5DPI (C-C''). Muscles are labeled with Mhc (magenta). (B'', C''). Boxed regions from (B and C), magnified 2X. Scale bars: 200 µm. **(D).** Quantification of tracheal coverage in (B) and (C) (****p < 0.0001, Student's t-test; n = 19 heminota per condition; light, dark, and intermediate shading indicate data points from three independent replicates). **(E).** Quantification of tracheal coverage in (C) at the injury site (orange box), adjacent to the injury site (green box, approximately 135 µm away from the injury site), and at distant regions (blue box, within 300 µm of the lesion border) (*p= 0.0142, Student's t-test; n=19 heminota). **(F-F').** dSRF-Gal4 marks muscle-associated terminal tracheal cells (TTCs). TTC membranes (green) and nuclei (magenta) are indicated by arrowheads and arrows, respectively (*dSRF-Gal4, UAS-mCD8GFP; UAS-H2B-RFP*). dSRF-Gal4 is inactive in primary tracheal branches (asterisks in F'). Muscles are labeled with Mhc (blue). Scale bars: 25 µm. **(G-H''').** TTCs distribution in IFMs (green, *dSRF-Gal4, UAS-mCD8GFP*) in control (G-G''') and at 5DPI (H-H'''). Muscles are labeled with Mhc (magenta).(G'',H''). 4.5X magnifications of boxed regions in (G') and (H'). Scale bar: 200 µm. (G''', H'''). Orthogonal views of (G'') and (H''). Arrow in (H''') indicates TTC enrichment at the injured muscle. **(I).** Quantification of TTCs coverage from (G) and (H) (****p < 0.0001, Student's t-test; n = 14 heminota per condition; light, dark, and intermediate shading points represent data points from three independent replicates). **(J-J').** dSRF (green) marks TTCs nuclei associated with IFMs. Scale bars: 25 µm. **(K-L''').** Distribution of TTCs nuclei (green) in IFMs under control conditions (K-K''') and at 5DPI (L-L'''). Muscles are labeled with phalloidin (blue); tracheae are visualized by autofluorescence (gray). Anti-PH3 (magenta) is used to assess cell division. (K', L'''). 2X magnification of boxed regions in (K) and (L). Scale bars: 100 µm. Arrowheads and arrows indicate dSRF expression in the muscle and TTCs nuclei, respectively. **(M).** Proportion of TTCs nuclei located within a selected muscle relative to the total number of TTCs nuclei in the imaged sample (*p = 0.036, Student's t-test; n = 17 heminota per condition; light, dark, and intermediate shading indicate data points from three independent replicates).

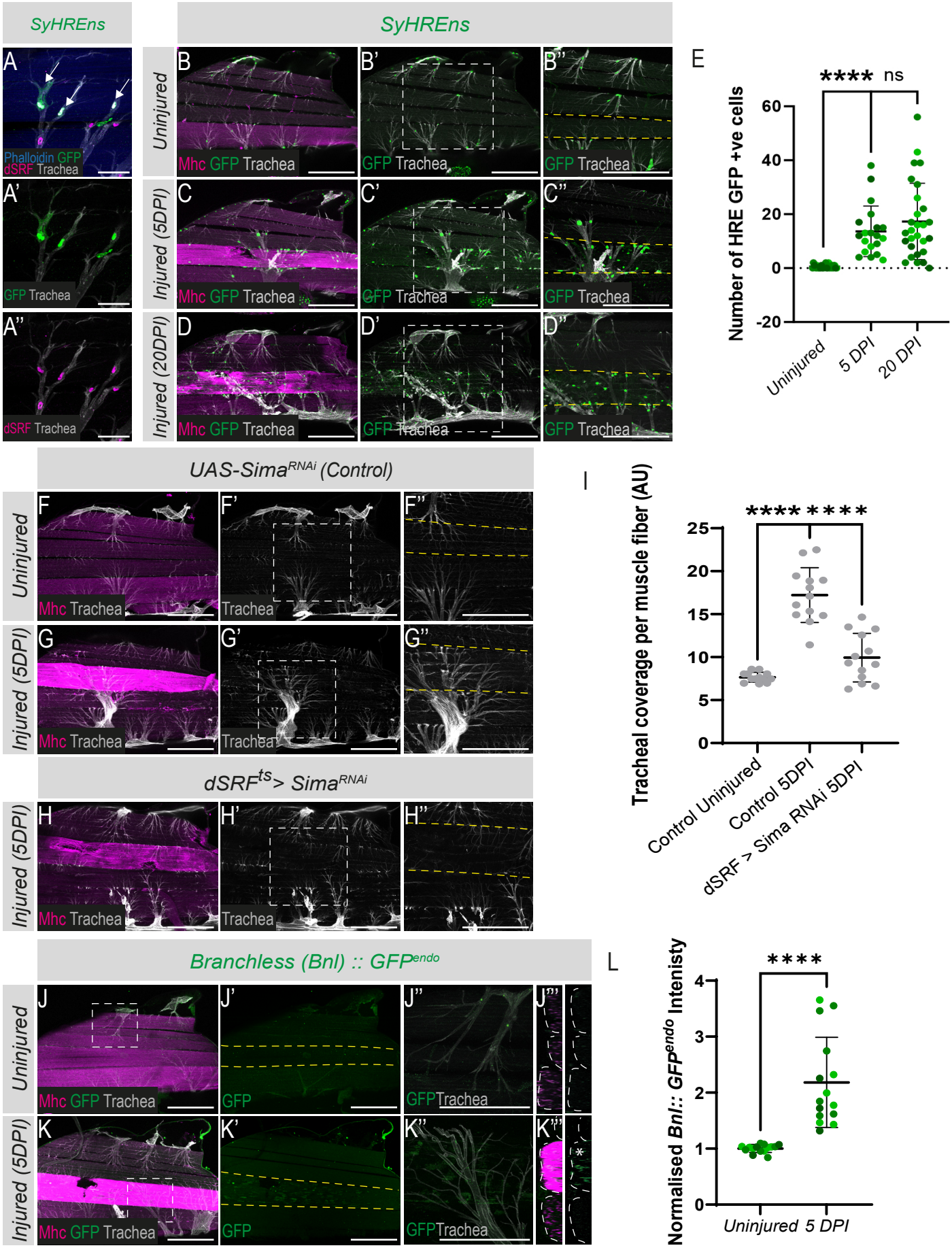
SyHREns
SyHREns
A
Phalloidin GFP
dSRF Trachea
A'
GFP Trachea
A''
dSRF Trachea
Uninjured
Injured (5DPI)
Injured (20DPI)
B
B'
B''
C
C'
C''
D
D'
D''
Mhc GFP Trachea
GFP Trachea
E
**** ns
Number of HRE GFP +ve cells
60
40
20
0
-20
Uninjured
5 DPI
20 DPI
UAS-Sima^RNAi (Control)
F
F'
F''
G
G'
G''
Mhc Trachea
Trachea
dSRF^ts> Sima^RNAi
H
H'
H''
I
Tracheal coverage per muscle fiber (AU)
**** ****
25
20
15
10
5
0
Control Uninjured
Control 5DPI
dSRF > Sima RNAi 5DPI
Branchless (Bnl) :: GFP^endo
J
J'
J''
J'''
K
K'
K''
K'''
Mhc GFP Trachea
GFP
GFPTrachea
L
Normalised Bnl:: GFP^endo Intenisty
****
4
3
2
1
0
Uninjured
5 DPI

Figure 3

Figure 3. Local hypoxia in response to muscle damage drives tracheal branching. (A-A''). *SyHREns* reporter activity (green) is detected in a subset of TTCs marked by dSRF (magenta, arrows). Scale bars: 25 µm. **(B-D'').** Expression of the *SyHREns* reporter (green) in control IFMs (B-B''), at 5DPI (C-C'') and 20DPI (D-D''). Muscles are labeled with Mhc (magenta), and tracheal branches are visualized via autofluorescence (gray). (B'', C'' and D''). 2X magnification of the boxed regions in B', C' and D'. Scale bars: 200 µm. **(E).** Quantification of SyHREns positive cells (green) per injured muscle fiber (****$p < 0.0001$, Student's t-test; $n > 20$ heminota per condition; light, dark and intermediate shading indicate data points from three independent replicates). **(F-H'').** Sima (HIF-1α) downregulation in TTCs (*dSRF-Gal4; UAS-Sima*^{RNAi}) prevents tracheal recruitment at the injured fiber. (F'', G'' and H''). 2X magnification of the boxed regions in E', F' and G'. Scale bars: 200 µm. **(I).** Quantification of trachea coverage (****$p < 0.0001$, Student's t-test; $n = 13$ heminota per condition). **(J-K'').** Detection of Bnl (green, *Bnl::GFP*^{endo}) in control IFMs (J-J'') and at 5DPI (K-K''). Muscles are labeled with Mhc (magenta), and tracheal cells are visualized via autofluorescence (gray). (J'', K''). 4.5X magnification of the boxed regions in J and K. Scale bars: 200 µm. (J''', K'''). Orthogonal views of (J) and (K). Asterisk in K''' indicates Bnl::GFP^{endo} enrichment at the injured muscle. **(L).** Quantification of normalized Bnl::GFP^{endo} intensity level in uninjured and injured muscle fiber at 5DPI (***$p<0.0001$, Student t-test, $n = 15$ heminota per condition from three independent replicates).

hs-Flp; SME-FRT-STOP-FRT-Gal4 ; UAS-Bnl::GFP, tubGal80^{ts}

Without Heat Shock | 2 hours Heat Shock + 1 Day at 30°C | 2 hours Heat Shock + 5 Days at 30°C

A, A', B, B', C, C'

dSRF GFP Trachea

Branchless (Bnl)-LacZ

Bnl :: GFP^{endo} , Pxn-RFP

Uninjured

Injured (5DPI)

D, D', D''

Mhc βGal DAPI

βGal

E, E', E''

F, F', F''

Mhc GFP RFP Trachea

GFP RFP

G, G', G''

Enh3 > mCD8GFP (Control)

H, H', H''

PhalloidinGFP Trachea

Trachea

I, I', I''

Enh3 > mCD8GFP ; Bnl^{RNAi}

J, J', J''

K

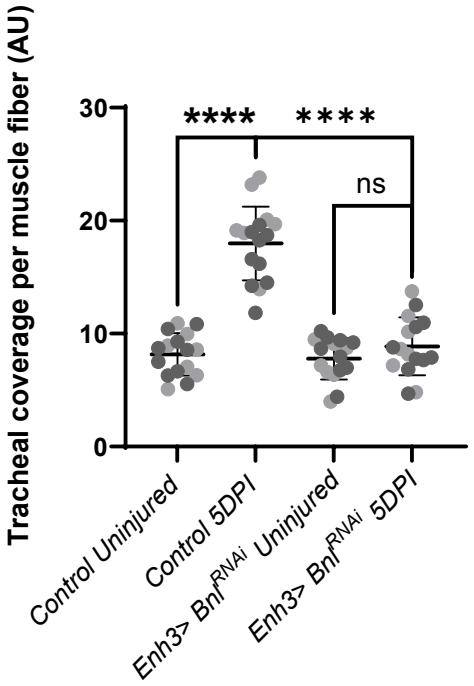

Flight assay

L

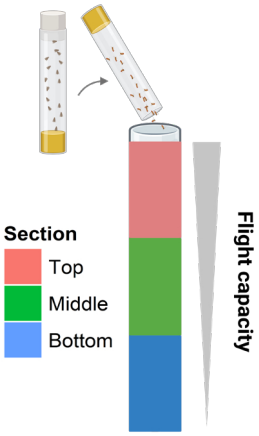

L'

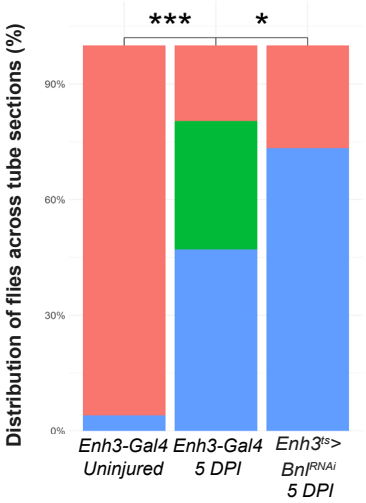

M

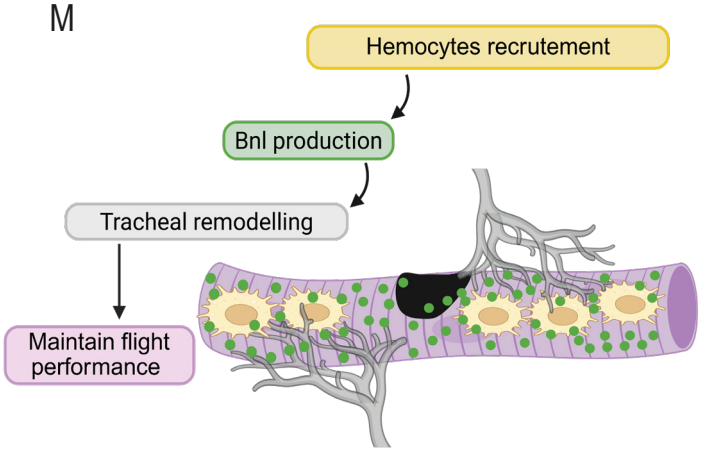

Figure 4

Figure 4. Hemocytes deliver Bnl to injured muscle to promote tracheal recruitment. (A-C'). Local overexpression of UAS-Bnl::GFP (green) in adult IFMs using *SME-Gal4* driver induces enrichment of terminal tracheal cells (TTCs; dSRF, magenta) and increases tracheal branching (gray), compared with controls (A). Scale bars: 200 µm. **(D-E'').** *Bnl-LacZ* reporter expression (green) is downregulated specifically in of the injured muscle fibers overexpressing Mhc (magenta), the nuclei are marked with DAPI (blue). (D', E''). 3.5X magnification of the boxed regions in D and E. Scale bars: 200 µm. **(F-G'').** Bnl expression (green, *Bnl::GFP*^{endo}) in uninjured IFMs (F-F'') and at 5DPI (G-G''). Muscles are labeled with Mhc (blue), tracheal cells visualized via autofluorescence (gray), and hemocytes detected with the *Pxn-RFP* reporter (magenta). Arrows in G'' indicate Bnl localization around hemocytes recruited to the injured muscle. Scale bars: 200 µm. **(H-J'').** Downregulating *bnl* in the hemocytes (green, *Enh3-Gal4; UAS-mCD8GFP, UAS-Bnl*^{RNAi}) do not alter hemocytes recruitment but decreases tracheal invasion to the damaged fiber as shown in (J'- J'') and quantified in **(K)** (**** $p < 0.0001$, Student t-test; $n = 16$ heminota from two independent replicates). Scale bars: 200 µm. **(L).** Schematic of the flight-assay setup used to assess flight performance. Flies are released at the top of a graduated cylinder, and landing position across three vertical zones is recorded. **(L').** Quantification of the proportion of flies distributed across three sections under three conditions: *Control Uninjured*, *Control Injured (5DPI)* and *Enh3-Gal4; UAS-Bnl*^{RNAi} *Injured (5DPI)*. Bars indicate the percentage of flies landing in each of the three flight-assay zones (***$p<0.001$, * $p < 0.05$ Chi-2 test). **(M).** Schematic model of hemocyte-driven tracheal recruitment required to maintain flight capacity following muscle injury.

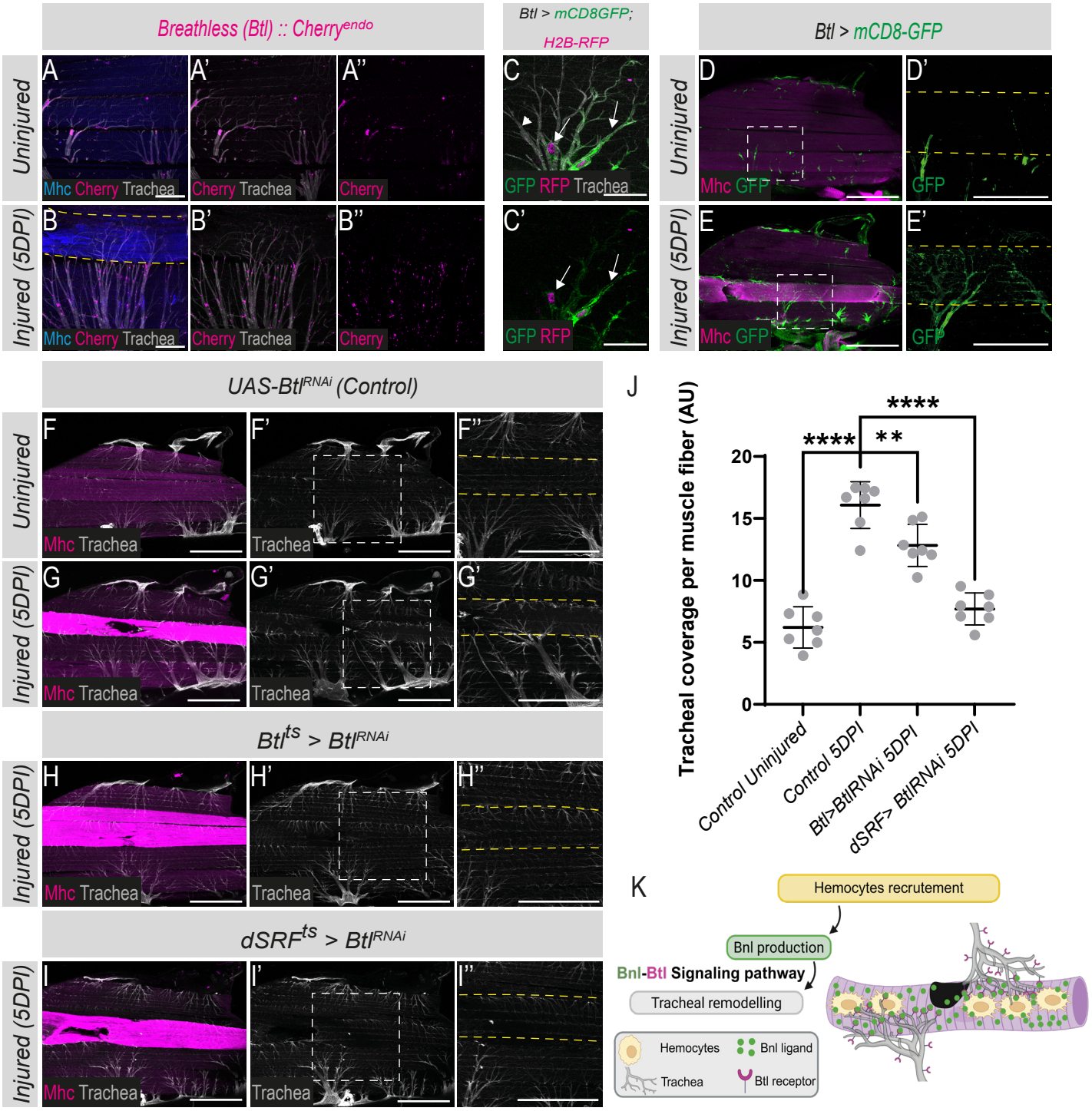
Breathless (Btl) :: Cherry^endo
Btl > mCD8GFP; H2B-RFP
Btl > mCD8-GFP
Uninjured
Injured (5DPI)
A
A'
A''
B
B'
B''
C
C'
D
D'
E
E'
Mhc Cherry Trachea
Cherry Trachea
Cherry
GFP RFP Trachea
GFP RFP
Mhc GFP
GFP
UAS-Btl^RNAi (Control)
Btl^ts > Btl^RNAi
dSRF^ts > Btl^RNAi
F
F'
F''
G
G'
G''
H
H'
H''
I
I'
I''
Mhc Trachea
Trachea
J
Tracheal coverage per muscle fiber (AU)
0
5
10
15
20
****
**
****
Control Uninjured
Control 5DPI
Btl>BtlRNAi 5DPI
dSRF> BtlRNAi 5DPI
K
Hemocytes recrutement
Bnl production
Bnl-Btl Signaling pathway
Tracheal remodelling
Hemocytes
Bnl ligand
Trachea
Btl receptor

Figure 5

Figure 5. The FGF receptor Breathless (Btl) is expressed along tracheal branches and is required for tracheal recruitment to the damaged muscle. (A-B''). Btl::Cherry^{endo} (magenta) is detected along tracheal branches (gray) associated with indirect flight muscles (IFMs) labelled with Mhc (blue), in either uninjured A or injured muscles B. Scale bars: 50 µm. Dashed yellow outlines indicate injured muscle fibers showing elevated Mhc expression. **(C-C').** The *Btl-Gal4* driver (green and magenta; *Btl-Gal4, UAS-mCD8GFP; UASH2B-RFP*) is active in a subset of tracheal branches (arrows, C-C'). Arrowheads in C indicate the tracheal branches that do not express the *Btl-Gal4* driver. Scale bars: 25 µm. **(D-E').** Activity of the *Btl-Gal4* driver (green, *Btl-Gal4, UAS-mCD8GFP*) in control (D) and at 5DPI (E). Muscles are labelled with Mhc (magenta). Scale bars: 200 µm. **(F-I'').** Downregulating *btl* in the tracheal cells with either *Btl-Gal4* driver (*Btl-Gal4; UAS-Btl^{RNAi}*, H-H'') or *dSRF-Gal4* driver (*dSRF-Gal4, UAS- Btl^{RNAi}*, I-I'') prevents tracheal invasion to the damaged fiber. **(J).** Quantification of trachea coverage (****p <0.0001, **p=0.0053, Student's t-test; n = 7 heminota per condition). Scale bars: 200 µm. **(K).** Schematic model of hemocyte-driven Bnl activates tracheal cells recruitment via Bnl/Btl signalling pathway.

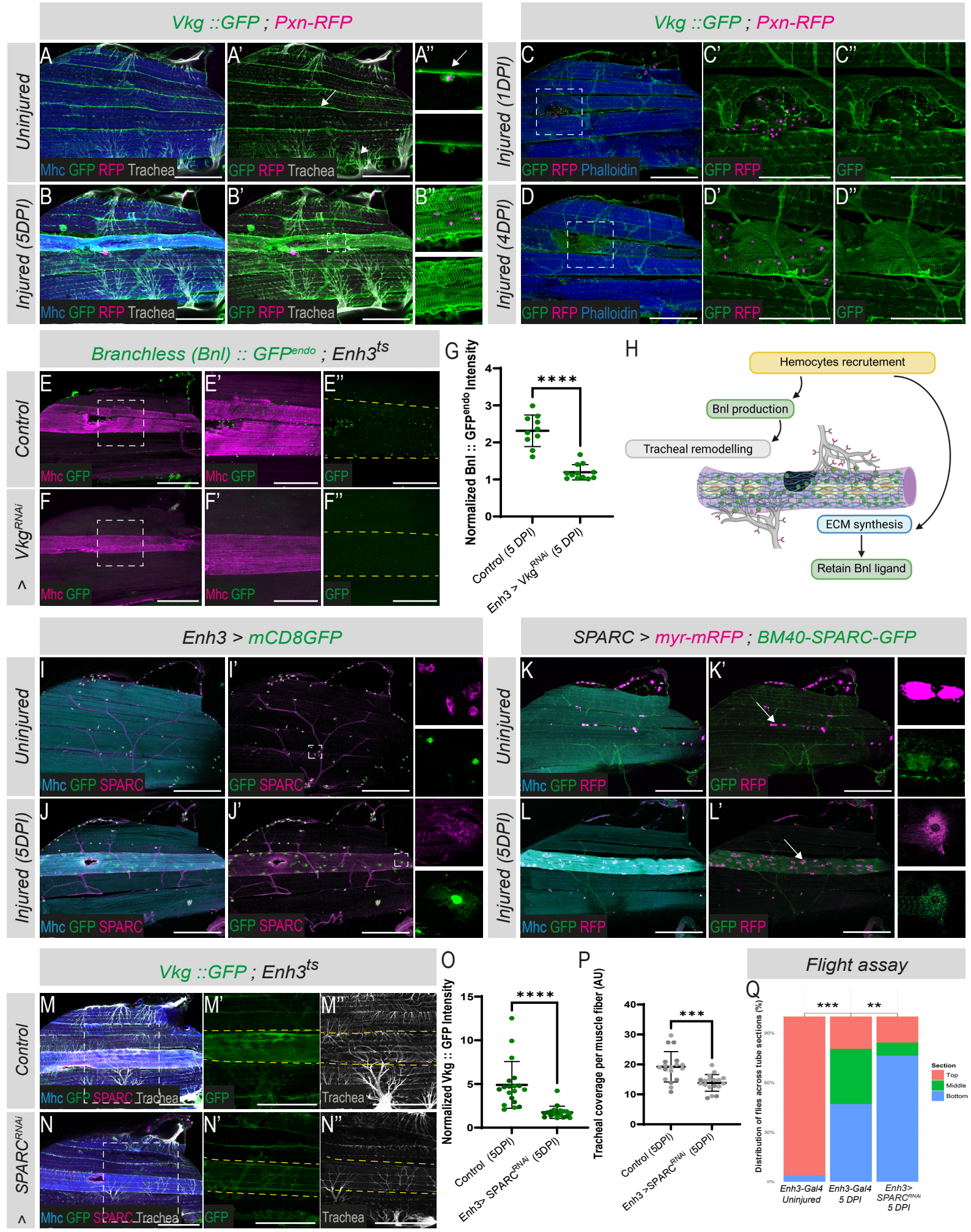
Vkg ::GFP ; Pxn-RFP
Uninjured
Injured (5DPI)
Mhc GFP RFP Trachea
GFP RFP Trachea
Injured (1DPI)
Injured (4DPI)
GFP RFP Phalloidin
GFP RFP
GFP
Branchless (Bnl) :: GFPendo ; Enh3ts
Control
Vkg RNAi >
Mhc GFP
Normalized Bnl :: GFPendo Intensity
****
Control (5 DPI)
Enh3 > VkgRNAi (5 DPI)
Hemocytes recrutement
Bnl production
Tracheal remodelling
ECM synthesis
Retain Bnl ligand
Enh3 > mCD8GFP
Mhc GFP SPARC
GFP SPARC
SPARC > myr-mRFP ; BM40-SPARC-GFP
Mhc GFP RFP
Vkg ::GFP ; Enh3ts
SPARC RNAi >
Normalized Vkg :: GFP Intensity
Control (5DPI)
Enh3> SPARCRNAi (5DPI)
Tracheal coverage per muscle fiber (AU)
***
Enh3 >SPARCRNAi (5DPI)
Flight assay
Distribution of flies across tube sections (%)
**
Section
Top
Middle
Bottom
Enh3-Gal4 Uninjured
Enh3-Gal4 5 DPI
Enh3> SPARCRNAi 5 DPI

Figure 6

Figure 6. Hemocytes deposit ECM components at injury muscles to constrain Bnl to damaged muscle fibers and maintain muscle function. (A-A''). Collagen IV (green, *Vkg::GFP*) is detected at basal levels around muscle fibers (arrow, A'), tracheal branches (arrowheads, A'), and hemocytes (magenta, *Pxn-RFP*; arrow, A'') in uninjured conditions. **(B-B'').** At 5DPI, Collagen IV is strongly enriched on the injured muscle fibers, labelled with Mhc (blue). **(C-D'').** Hemocytes recruitment (magenta, *Pxn-RFP*) and Collagen IV (green, *Vkg::GFP*) distribution on the injured muscle, at 1DPI and 4DPI. Scale bars: 200 µm. **(E-F″).** Endogenous Bnl (green, *Bnl::GFP*^{endo}) is enriched along damaged muscle fibers (magenta, Mhc) and is markedly reduced upon hemocyte-specific depletion of Collagen IV (*Enh3-Gal4, UAS-Vkg*^{RNAi}). **(G).** Quantification of normalized Bnl intensity in injured fibers (****p<0.0001, Student t-test, n = 13 heminota per condition). **(H).** Schematic model of hemocyte-mediated ECM delivery required to confine Bnl to injured muscle fibers. **(I-I').** SPARC (magenta) is detected in the IFMs associated hemocytes visualized by *Enh3-Gal4* driver (green, *Enh3-Gal4, UAS-mCD8GFP*). **(J-J').** SPARC expression is increased in injured fibers compared to controls (I-I'). **(K-K').** Adult hemocytes (magenta; *SPARC-Gal4, UAS-myr-RFP*) express BM40-SPARC-GFP (green). **(L-L').** BM40-SPARC-GFP produced by adult hemocytes is broadly distributed along the injured muscle fibers. **(M-N').** Downregulation of *SPARC* in adult hemocytes (*Enh3-Gal4 > UAS-SPARC*^{RNAi}) reduces Collagen IV enrichment (green, *Vkg::GFP*) and impairs tracheal recruitment in injured fiber (gray, autofluorescence), as quantified in panels **(O)** and **(P)** respectively (O. ****p<0.0001, Student t-test, n = 20 heminota per condition from two independent replicates, P. ***p<0.001, Student t-test, n = 18 heminota per condition from two independent replicates). **(Q).** Quantification of the proportion of flies distributed across three sections (Top, Middle and Bottom) under three conditions: *Control Uninjured*, *Control Injured (5DPI)* and *Enh3-Gal4; UAS-SPARC*^{RNAi} *Injured (5DPI)* (***p<0.001, ** p < 0.01 Chi-2 test).

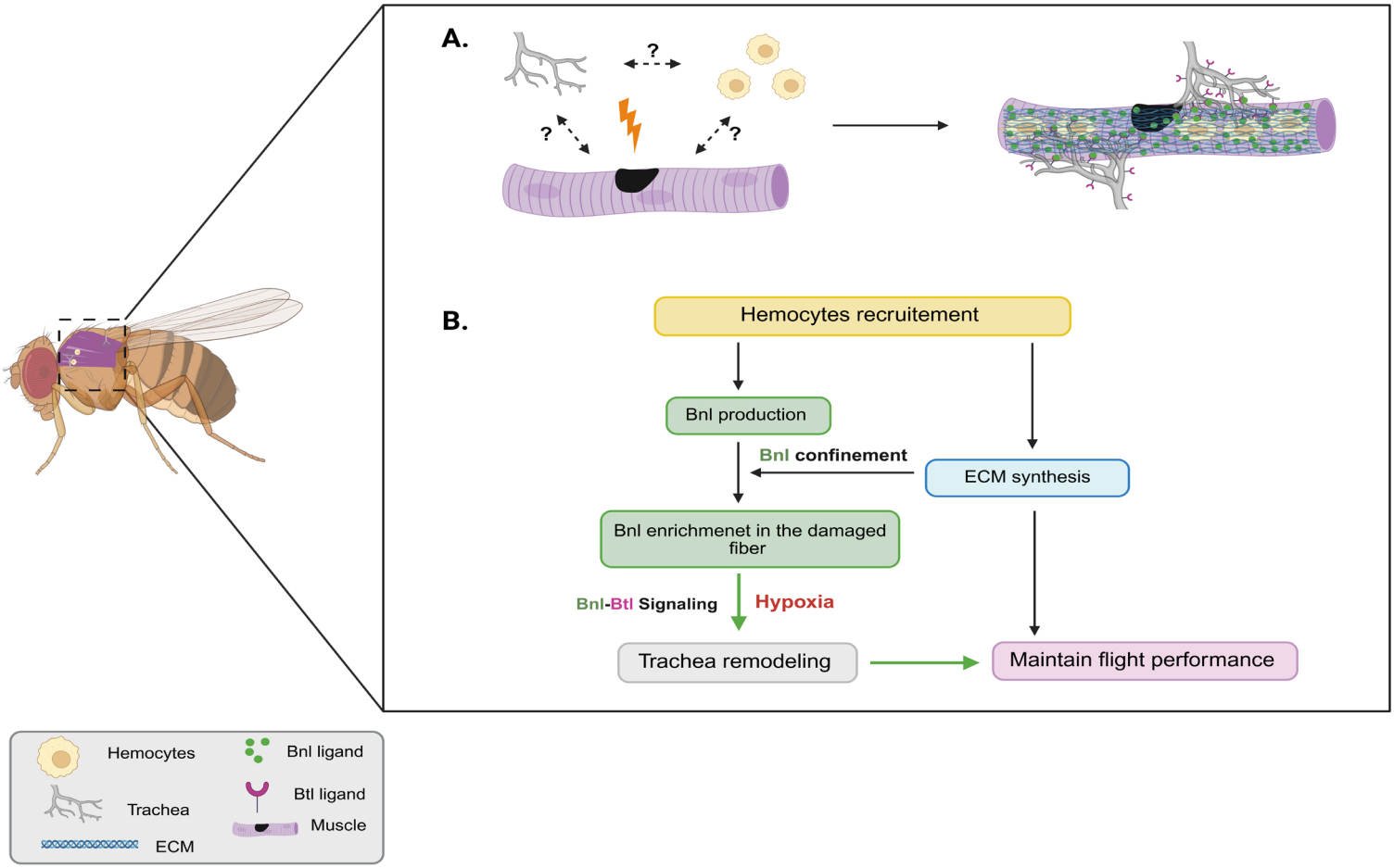
A.
?
?
?
B.
Hemocytes recruitement
Bnl production
Bnl confinement
ECM synthesis
Bnl enrichmenet in the damaged fiber
Bnl-Btl Signaling
Hypoxia
Trachea remodeling
Maintain flight performance
Hemocytes
Bnl ligand
Btl ligand
Trachea
Muscle
ECM

Figure 7

Figure 7. Hemocyte-muscle-tracheal intercellular signaling orchestrates tracheal remodelling and muscle repair after injury. (A). Schematic representation of the hemocyte-muscle-tracheal signaling module activated in response to muscle injury. **(B).** Upon muscle damage, hemocytes are rapidly recruited to the injured fiber, where they secrete the FGF ligand Branchless (Bnl), which activates its receptor Breathless (Btl) on tracheal cells. Bnl–Btl signaling drives tracheal remodeling and directional outgrowth toward the injured muscle. In parallel, hemocytes deposit extracellular matrix (ECM) components that retain Bnl and stabilize trachea-muscle attachments. Together, these coordinated cellular mechanisms promote muscle repair and preserve flight performance.

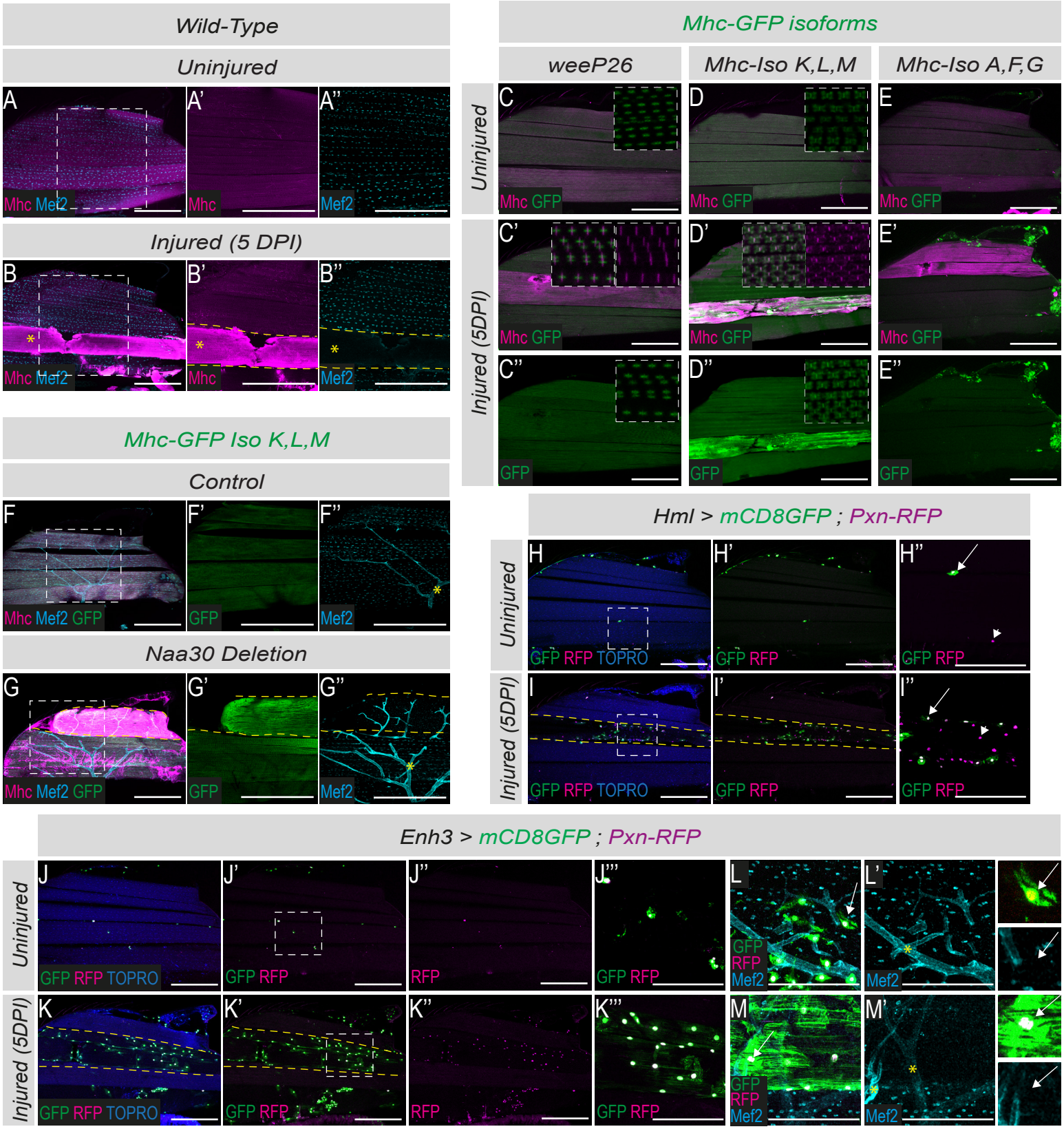
Wild-Type
Uninjured
A
A'
A''
Mhc Mef2
Mhc
Mef2
Injured (5 DPI)
B
B'
B''
Mhc Mef2
Mhc
Mef2
Mhc-GFP isoforms
weeP26
Mhc-Iso K,L,M
Mhc-Iso A,F,G
Uninjured
Injured (5DPI)
C
D
E
C'
D'
E'
C''
D''
E''
Mhc GFP
GFP
Mhc-GFP Iso K,L,M
Control
F
F'
F''
Mhc Mef2 GFP
GFP
Mef2
Naa30 Deletion
G
G'
G''
Mhc Mef2 GFP
GFP
Mef2
Hml > mCD8GFP ; Pxn-RFP
Uninjured
Injured (5DPI)
H
H'
H''
I
I'
I''
GFP RFP TOPRO
GFP RFP
Enh3 > mCD8GFP ; Pxn-RFP
Uninjured
Injured (5DPI)
J
J'
J''
J'''
L
L'
K
K'
K''
K'''
M
M'
GFP RFP TOPRO
GFP RFP
RFP
GFP
Mef2

Figure S1

Supplementary data

Figure S1. Mhc upregulation marks the damaged muscle fiber. (A-B''). IFMs stained for Mhc (magenta) and Mef2 (cyan) show upregulation of Mhc and downregulation of Mef2 in the injured fiber (asterisks, B'-B'') at 5DPI, compared to the control (A'-A''). (A', B'). 2X magnification of the boxed regions in A and B. Scale bars: 200 µm. **(C-C'').** Expression of the embryonic Mhc isoform (*weeP26*, green) in uninjured (C) and injured (C'-C'') IFMs. Injury does not alter weeP26 expression (C and C''). **(D-D'').** The shorter Mhc isoforms (*Mhc-Iso-K, L, M (fTRG500)*; green) colocalize with anti-Mhc staining (magenta) and are upregulated in injured muscle (D'-D''). **(E-E'').** The longer Mhc-GFP isoforms (*Mhc-Iso-A, F, G (fTRG519)*; green) are not expressed in adult IFMs and are not upregulated in response to muscle injury (E'-E''). Scale bars: 200 µm. **(F-G'').** In *Naa30A mutant* IFMs, defective muscle attachment correlates with increased Mhc expression (magenta, G), upregulation of short Mhc-GFP isoforms (green, G'), and a loss of Mef2 (cyan, G''). **(H-I'').** Co-expression of hemocytes markers *HmlΔ-Gal4, UAS-mCD8GFP* (green) and *Pxn-RFP* (magenta) reveals two subsets of hemocytes associated with the IFMs: Pxn+Hml+ (arrows) and Pxn+Hml- (arrowheads). Nuclei are visualized with TO-PRO (blue). Data from n >10 heminota from two independent replicates. Scale bars: 200 µm. (H''-I''). 3X magnification of the boxed regions in H and I. Scale bars: 100 µm. **(J-M').** Co-expression analysis of *Enh3-Gal4; UAS-mcD8GFP* (green) and *Pxn-RFP* (magenta) shows that all Enh3+ cells express Pxn (J'-K'). No Mef2 expression (cyan) is observed in these cells, in either undamaged (L') or damaged (M', dashed lines) fibers. Scale bars: 200 µm. Yellow asterisks in panels F', G'' and L' mark non-specific signal detected in motoneurons.

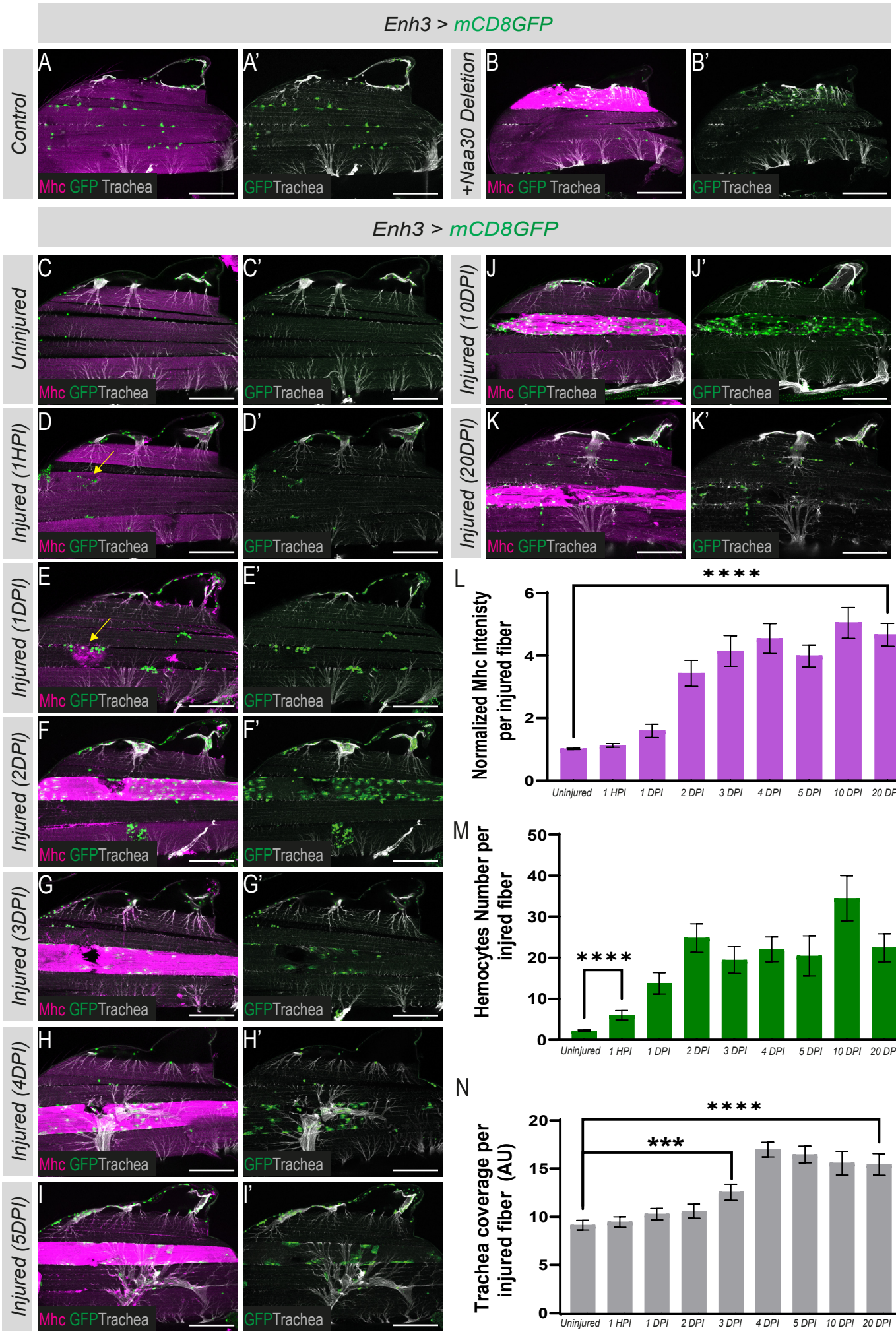
Enh3 > mCD8GFP
Control
+Naa30 Deletion
A
A'
B
B'
Mhc GFP Trachea
GFP Trachea
Enh3 > mCD8GFP
Uninjured
Injured (1HPI)
Injured (1DPI)
Injured (2DPI)
Injured (3DPI)
Injured (4DPI)
Injured (5DPI)
Injured (10DPI)
Injured (20DPI)
C
C'
D
D'
E
E'
F
F'
G
G'
H
H'
I
I'
J
J'
K
K'
L
Normalized Mhc Intenisty per injured fiber
****
Uninjured
1 HPI
1 DPI
2 DPI
3 DPI
4 DPI
5 DPI
10 DPI
20 DPI
M
Hemocytes Number per injred fiber
****
N
Trachea coverage per injured fiber (AU)
***
****

Figure S2

Figure S2. Early recruitment of hemocytes initiates tracheal remodeling after muscle damage. (A-B'). In *Naa30A mutant* flies, defective muscle attachment is associated with tracheal enrichment (gray, B') and increased hemocytes accumulation (green, B') compared to controls (A-A'). **(C-K').** Time-course analysis of tracheal remodeling and hemocytes recruitment in *Enh3-Gal4; UAS-mCD8GFP* adult IFMs following localized stab injury. Tracheal branches are visualized by autofluorescence (gray), and hemocytes are labeled with GFP (green). Muscles are labeled with Mhc (magenta). Time points range from 1-hour post-injury (1HPI) to 20 days post-injury (20DPI). **(L).** Quantification of normalized Mhc intensity. **(M).** Quantification of the hemocytes number in the injured fiber shows a significant increase starting at 1HPI which remains elevated until 20DPI. **(N).** Tracheal quantification shows a marked increase in its density from 3DPI and remains sustained until 20 DPI. (****$p < 0.0001$, ***$p < 0.001$; Student's t-test; $n \geq 10$ heminota per condition). Scale bars: 200 µm.

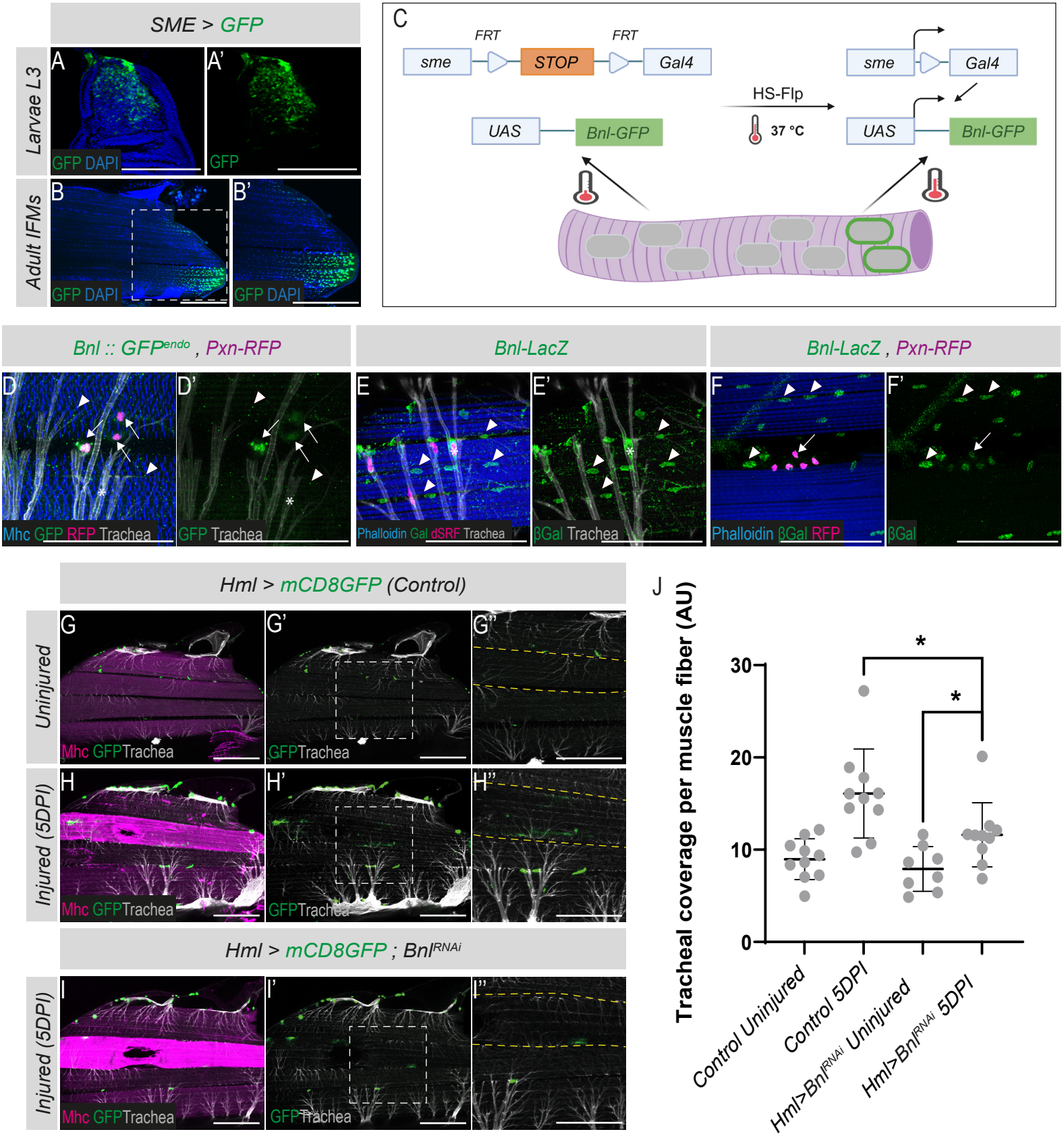
SME > GFP
Larvae L3
Adult IFMs
A
A'
B
B'
GFP DAPI
GFP
C
FRT
FRT
sme
STOP
Gal4
HS-Flp
37 °C
UAS
Bnl-GFP
Bnl :: GFPendo , Pxn-RFP
Bnl-LacZ
Bnl-LacZ , Pxn-RFP
D
D'
E
E'
F
F'
Mhc GFP RFP Trachea
GFP Trachea
Phalloidin Gal dSRF Trachea
βGal Trachea
Phalloidin βGal RFP
βGal
Hml > mCD8GFP (Control)
Uninjured
Injured (5DPI)
G
G'
G''
H
H'
H''
Mhc GFPTrachea
GFPTrachea
Hml > mCD8GFP ; BnlRNAi
I
I'
I''
J
Tracheal coverage per muscle fiber (AU)
30
20
10
0
*
*
Control Uninjured
Control 5DPI
Hml>BnlRNAi Uninjured
Hml>BnlRNAi 5DPI

Figure S3

Figure S3. Tracheal branching requires precise control of Bnl provided by the hemocytes. (A-B'). Expression pattern of the Shavenbaby (Svb) muscle regulatory enhancer (SME) (green, *SME-Gal4; UAS-mCD8GFP*). SME-Gal4 drives GFP expression (green) in a subset of larval muscle progenitors located in the posterior region of the wing disc (A-A') and in a subset of adult muscle nuclei (green and blue (DAPI), B-B'). Scale bars: 200 µm. **(C).** Schematic representation of the FLP-OUT system used to drive UAS-Bnl::GFP expression in a subset of adult muscle nuclei, using the *Hs-FLP; FRT-SME-Stop-FRT-Gal4/CyO; tub-Gal80ts* combination. **(D-D').** Bnl (green, *Bnl::GFP*^{endo}) is detected in indirect flight muscles (IFMs, labelled with Mhc, blue; arrowheads), tracheal branches (autofluorescence, gray; asterisks), and hemocytes (*Pxn-RFP*, magenta; arrows). Scale bars: 25 µm. **(E-E').** Expression of the *Bnl-LacZ* reporter (green) is observed in terminal tracheal cells (TTCs) marked by dSRF (magenta; asterisks), and in IFMs nuclei (arrowheads). Scale bars: 25 µm. **(F-F').** Bnl-LacZ (green) is detected in IFMs associated hemocytes labelled with *Pxn-RFP* (magenta; arrows). Scale bars: 25 µm. **(G-I'').** Targeted downregulation of *bnl* in a subset of hemocytes using *HmlΔ-Gal4* driver significantly reduces tracheal enrichment at the injured fiber, as quantified in **(J).** (*$p < 0.05$, Student's t-test; $n \geq 10$ heminota per condition). Scale bars: 200 µm.

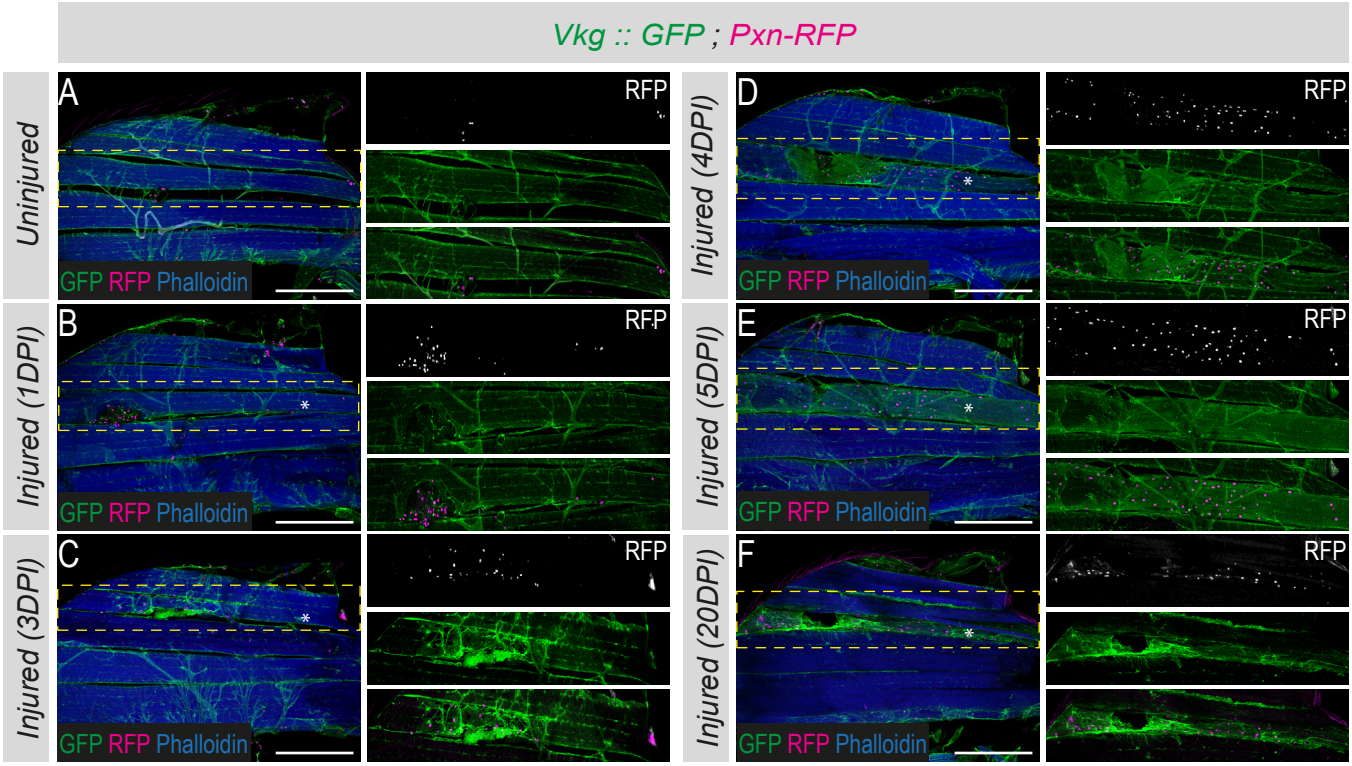
Vkg :: GFP ; Pxn-RFP
Uninjured
Injured (1DPI)
Injured (3DPI)
Injured (4DPI)
Injured (5DPI)
Injured (20DPI)
A
B
C
D
E
F
RFP
GFP RFP Phalloidin

Figure S4

Figure S4. Time-course analysis of hemocyte recruitment and Collagen IV deposition following muscle injury. (A-F). Hemocyte recruitment (magenta, *Pxn-RFP*) and Collagen IV distribution (green, *Vkg::GFP*) in uninjured muscles (A) and at successive time points after injury (B-F), from 1 to 20 days post injury (DPI). Scale bar: 200 µm.